UNIVERSIDAD CARLOS III DE MADRID

School of Engineering

Bachelor's Degree in Aerospace Engineering

EFFECT OF BASE FLOW NON-PARALLELISM ON THE LOCAL LINEAR STABILITY OF LOW-DENSITY JETS

Bachelor Thesis

Author
José Miguel Blanco Iglesias

Advisor
Wilfried Coenen

Department of Fluid Mechanics and Thermal Engineering

Leganés, June 2014

Department of Fluid Mechanics and Thermal Engineering
School of Engineering

Bachelor's Degree in Aerospace Engineering

EFFECT OF BASE FLOW NON-PARALLELISM ON THE LOCAL LINEAR STABILITY OF LOW-DENSITY JETS

Bachelor Thesis

Author
José Miguel Blanco Iglesias

Thesis advisor
Wilfried Coenen

Leganés, June 2014

To my family and Irene

Acknowledgements

First of all, I would like to thank Antonio Sanchez, who made possible that I started collaborating with the Department of Fluid Mechanics in what would later become this thesis. That is how I met Wilfried Coenen, my thesis advisor. I truly appreciate his help and guidance in the completion of this thesis.

The present work means the culmination of an important period of my life. Therefore, I would like to take advantage of this opportunity to thank all those people that have made it such an unforgettable experience.

To my classmates, that now are much more than that. After this four years I can proudly say they are my friends. Alvaro, Maria, Nico, Lorena, Maria, Kuc, Pablo, Eric, Alvaro, Diego, Sergio, Guille and all of you, the first generation of Aerospace Engineers at Universidad Carlos III, because the countless hours of hard work bring people closer, but enjoying time with each other is what sticks them together. Thank you all for those great moments.

To Alba, Gema, Celia, Pepi and that big family that is the residence hall Fernando Abril Martorell. Living with you has been delightful.

To my professors, Manolo, Oscar, Antonio, Manuel, Jesus, Concha, and all of you that have given me class, someone said once that we are just dwarfs standing on the shoulders of giants, thank you for helping us getting up there.

To Angelines, Dioni, Pepe, Almudena, Alberto, my family here in Leganes, thanks for this wonderful years.

To Pablo, Javi and Alberto and the people of the group from Badajoz, because of people like you it is tough to live far from home.

To Irene, it is curious how we don't realize it, but you have been there since I started university four years ago. Thanks for everything.

To my family, for your care and support not just this four years, but throughout my whole life. I would not be who I am today if it were not for you.

I could not have wished for better people to share my way. Thank you all again.

Jose Miguel Blanco Iglesias, June 2014

Abstract

The effect of retaining base flow non-parallelism in the local linear spatiotemporal stability analysis of slender low-density jets, discharging from a round injector into a quiescent ambient, is studied in the present work.

Retaining base flow non-parallelism in the local linear stability analysis was found to have a stabilizing effect in the flow closer to the injector exit. This effect was greater the lower the values of the Reynolds number and the initial momentum thickness of the velocity profile at the injector exit.

When comparing the results obtained to existing experimental data, maintaining the base flow non-parallelism in the analysis gave better agreement with the experimental data than not taking base flow non-parallelism into account. Furthermore, it changed the evolution of the local stability properties so that a more theoretically sound criteria could be used in determining the absolute or convective unstable nature of the flow. This allows to reduce the uncertainty in the stability description of the flow when base flow non-parallelism is retained in the stability analysis.

Contents

CHAPTER

ONE

Introduction

Instabilities in low-density jets

A jet is a stream of fluid (liquid or gas) being forced out of a small opening. In particular, we will consider jets discharging into a stagnant atmosphere. This kind of flow presents a high streamwise shear component, that dominates the flow, between the moving fluid and the stagnant atmosphere. The study of the behavior of jets to perturbations became of particular interest when jet propulsion became possible, due to the high noise generation of jet engines, but jets are present as well in combustion processes and mixing of fluids among other fields. The response to instabilities of low-density jets specifically shows certain characteristics that made them subject to detailed study.

Low-density jets are those jets whose density is smaller than the ambient value. This can be achieved in two manners, that we will denominate hot and light jets. Hot jets are those in which the jet and the atmosphere it discharges to consist of the same species, but the jet is at a higher temperature. Light jets, on the contrary, are isothermal but the species of the jet and the ambient are different, being the species of the jet of a lower density, for example helium jet discharging into an air atmosphere.

Related to the instability of jets, two types of behavior can be observed. Jets can act as noise amplifiers or present self-excited oscillations. Constant density jets and low-density jets at sufficiently small Reynolds numbers are known to behave as noise amplifiers. In this type of behavior perturbations grow in time but they are carried away downstream. Low-density jets, under certain conditions, present self-excited oscillations where certain frequencies dominate the flow. In this cases perturbations are able to propagate upstream, contaminating the whole flow and triggering a global instability mode so that the oscillation of the whole jet is synchronized at a certain dominant frequency. In figure 1.1 both type of behaviors are shown for a low-density jet. We can observe a considerable increase in the spreading of the jet for the case in which self-oscillations are present. A spectrum analysis of that jet for the two different conditions

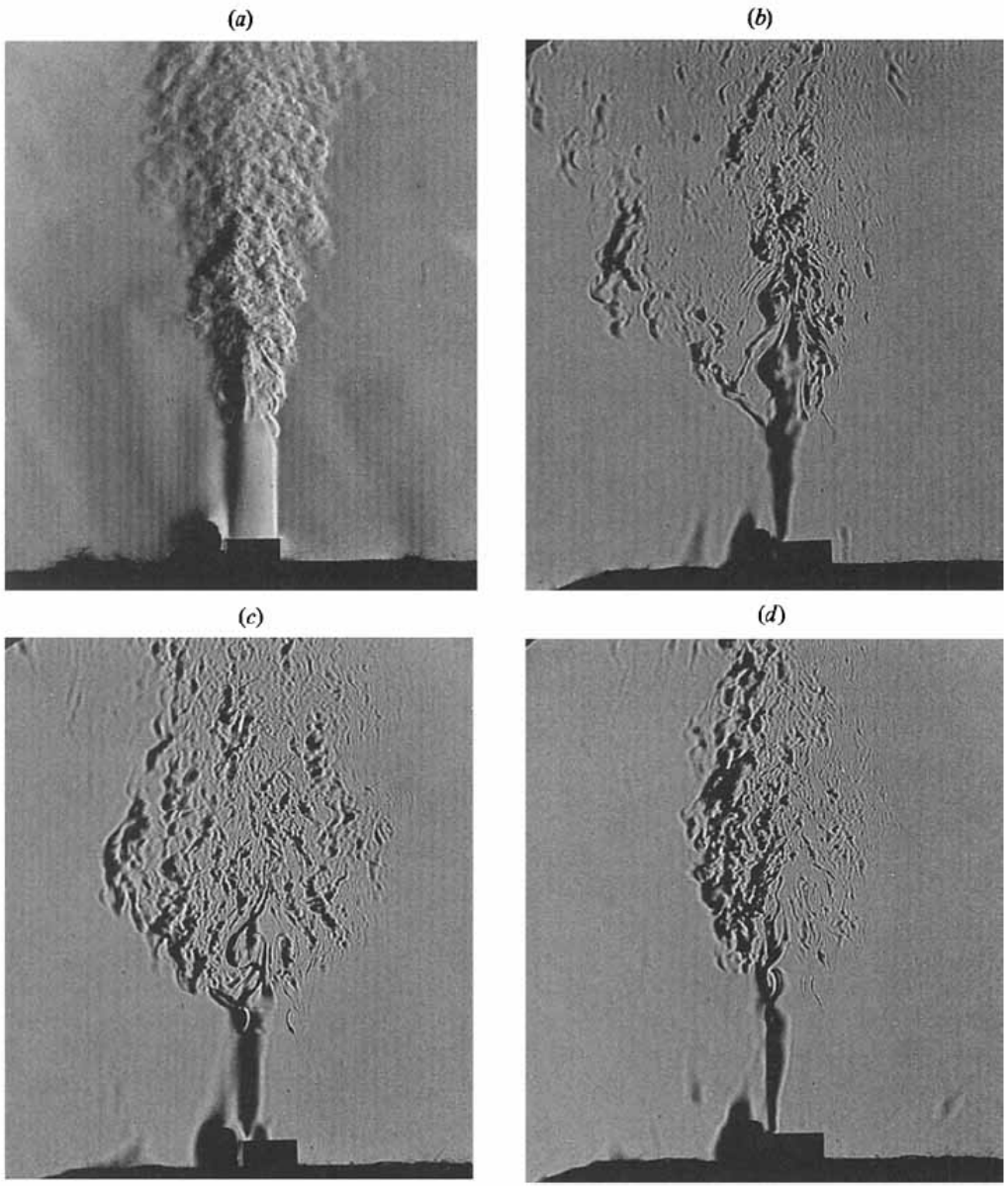

Figure 1.1: Spark schlieren views of a hot jet. (a) Shows a slightly heated jet ($T = 50C$) with a density ratio $S = \rho_j/\rho_\infty = 0.91$ and $Re = 10^4$ behaving as a noise amplifier whereas (b),(c)and (d) show different views of the same jet with a density ratio of $S = 0.62$, $T_j = 200$ and $Re = 7500$, presenting self-excited oscillations. Figure taken from Monkewitz *et al.* (1990).

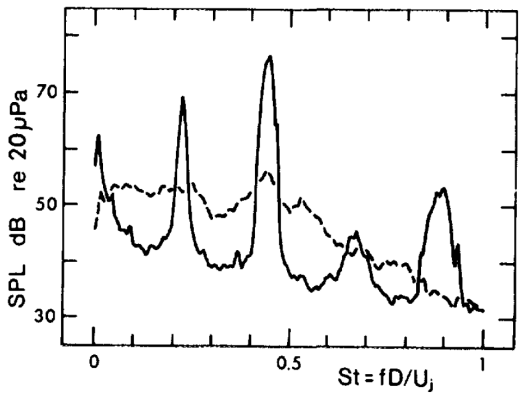

Figure 1.2: Near-field pressure spectrum obtained for a hot jet with $S = \rho_j/\rho_\infty = 0.47$ (solid line) and a constant density jet, $S = 1$ (dashed line). Figure taken from Monkewitz *et al.* (1989).

would show something qualitatively similar to the spectrum shown in figure 1.2. The spectrum for a hot jet and a constant density jet at similar dynamic characteristics is shown in that figure. It can be observed that for the constant density jet the spectrum is a somewhat smooth curve. Whereas for the hot jet the flow shows certain strongly dominant frequencies.

Literature review

A first look into the underlying physical phenomena inherent to (the stability of) free shear flows, of which jets are a subset, can be found in the seminal works of Helmholtz (1868),Kelvin (1871) and Rayleigh (1880). Many efforts have been dedicated since then to understanding the dynamics of this kind of flows.

In particular, the response of constant density jets to small perturbations has been widely studied (see for instance Batchelor & Gill (1962),Reynolds (1962),Kambe (1969),Lessen & Singh (1973),Mollendorf & Gebhart (1973),Mattingly & Chang (1974),Morris (1976),Cohen & Wygnanski (1987)).

However, low-density jets present intrinsic dynamics in opposition to constant density jets. This is due to a physical phenomenon that is specific to low-density jets, the baroclinic torque. The baroclinic torque is related with the generation of vorticity due to a mismatch in gradients of pressure and density that does not exist in the case of a constant density jet. It has been shown to play an important role in the onset of instability in low-density jets (Lesshafft & Huerre (2007)).

The oscillatory behavior of low-density jets is associated with the concept of

absolute instability. Absolute and convective instability terms refer to whether the perturbations are able to travel upstream and contaminate the whole flow or are just carried away downstream. These stability concepts were first developed by plasma physicist halfway through the 19th century (Twiss (1951),Twiss (1952),Landau & Lifschitz (1954),Sturrock (1958)) and then introduced by fluid mechanics researchers (Gaster (1968),Tam (1971),Huerre & Monkewitz (1985)). The concepts of absolute and convective instability are local concepts. However, the distribution of local instability properties and the global instability of the flow are closely related in slowly spatially developing flows (see Huerre & Monkewitz (1990);Chomaz (2005)). Specifically, small pockets of local instability have been shown to trigger global instability modes in jets (see the work of Lesshafft *et al.* (2006),Lesshafft & Huerre (2007), who performed complete numerical simulations of the flow). This allows to perform a local stability analysis rather than a more complex global analysis to predict the global stability properties, decreasing in this manner the computational cost associated to the analysis.

The phenomenon of self-sustained oscillations in low-density jets has been observed experimentally by Sreenivasan *et al.* (1989),Kyle & Sreenivasan (1993), Hallberg & Strykowski (2006) in the case of helium/air mixtures and by Monkewitz *et al.* (1990),Raghu & Monkewitz (1991) in the case of heated air. Moreover, the local stability of the near field of low-density jets has been studied theoretically in numerous occasions (see for instance Monkewitz (1988),Yu & Monkewitz (1990)Jendoubi & Strykowski (1994),Sevilla *et al.* (2002),Lesshafft & Huerre (2007).Hallberg *et al.* (2007),Nichols *et al.* (2007),Srinivasan *et al.* (2010),Coenen & Sevilla (2012)).

Local linear hydrodynamic stability analysis

Temporal and spatial stability theories independently fail to grasp the stability properties of low-density jets. Therefore, when studying the stability of that type of flow, a spatiotemporal stability analysis is desired. In a spatiotemporal stability analysis, perturbations of a determined shape are introduced into the equations of motion. Those perturbations are allowed to grow and fade both in space and time. The parameter related with the behavior in time is the frequency, ω, and the one related with the behavior in space is the wavenumber, k, both complex. In a spatiotemporal stability analysis both are interrelated. Specifically, when solving the stability equations only certain combinations of k and ω satisfy them. In order to obtain the local stability properties, the values of k and ω are computed for the wave packet of zero velocity (ω_0, k_0) at each streamwise location of the flow. The wave packet of zero velocity represents the

perturbations that stay at the source. If those perturbations grow in time, which is determined by a positive value of the imaginary part of ω_0, the flow is said to be locally absolutely unstable at that point. On the contrary, if perturbations die eventually ($\omega_{0,i}<0$) the flow is said to be locally convectively unstable there. Once the evolution of the local stability properties of the flow is obtained, the global stability of the flow can be inferred from it, as was already mentioned before.

Motivation

Typically, when studying the stability of slender low-density jets at moderately high Reynolds numbers, the analysis is performed neglecting base flow terms that are not strictly parallel in the equations of motion. Namely, those terms are the radial velocity component and the axial derivatives of the base flow. They are considered an order of magnitude smaller than other base flow properties, like the axial velocity, when compared directly. However, when those base flow non-parallel terms are retained into the equations of motion and an order of magnitude analysis is performed, it can be observed that some of the terms containing base flow non-parallelism remain of equivalent significance as strictly parallel terms of the base flow. The main motivation of the present work is to study the effect base flow non-parallelism in the stability characteristics of low-density jets.

The stability analysis performed in the present work specifically involves hot jets. However, the trends identified in here for hot jets are believed, due to a similar structure of the flow, to be applicable to light jets.

Alternative approaches

There are different approaches to understand the global stability of the flow. One of them is to perform a local linear stability analysis as the one developed in the present work. With this method the stability properties are computed at a local level and then from the distribution of local properties the global behavior is inferred. Another option consist in performing a direct global stability analysis. In this case, ulike in the local linear stability analysis, the spatial shape of the perturbation is an unkonwn that will be solved for in the analysis. However, this option would increase the complexity of the underlying numerical tools used as now the computational domain is the whole flow, and not just radial planes at each streamwise location as in the case of a local linear stability analysis. Furthermore, a complete Direct Numerical Simulation (DNS) can be performed, thus increasing exponentially the computational cost of the analy-

sis. Finally, a set of experiments may be conducted. This option needs special facilities and a very careful set-up. As mentioned before, this type of flow is very sensitive to perturbation and thus a car passing by the building in which the experiment is being performed would corrupt the data obtained.

1.1 Outline of the dissertation

Chapter 2 presents the theoretical background. The obtention of the base flow and the spatiotemporal stability analysis performed are described there. Then, in chapter 3 we present an overview of the procedure needed to compute the desired local stability properties of the flow. In chapter 4 the results are shown and discussed. Finally, chapter 5 holds the conclusions and future prospects. In the appendix A, a brief overview of the numerical methods used for the computation of the results is given.

References

Batchelor, G. K. & Gill, A. E. 1962 Analysis of the stability of axisymmetric jets. *J. Fluid Mech.* **14**, 529–551.

Chomaz, J. M. 2005 Global instabilities in spatially developing flows: Non-normality and nonlinearity. *Ann. Rev. Fluid Mech.* **37**, 357–392.

Coenen, Wilfried & Sevilla, A. 2012 The structure of the absolutely unstable regions in the near field of low-density jets. *J. Fluid Mech.* **713**, 123–149.

Cohen, J. & Wygnanski, I. 1987 The evolution of instabilities in the axisymmetrical jet. Part 1. The linear growth of disturbances near the nozzle. *J. Fluid Mech.* **176**, 191–219.

Gaster, M. 1968 Growth of disturbances in both space and time. *Phys. Fluids* **11**, 723–727.

Hallberg, M. P., Srinivasan, V., Gorse, P. & Strykowski, P. J. 2007 Suppression of global modes in low-density axisymmetric jets using coflow. *Phys. Fluids* **19** (1), 014102.

Hallberg, M. P. & Strykowski, P. J. 2006 On the universality of global modes in low-density axisymmetric jets. *J. Fluid Mech.* **569**, 493–507.

Helmholtz, H. von 1868 Über discontinuirliche Flüssigkeitsbewegungen. *Monats. Königl. Preuss. Akad. Wiss. Berlin* **23**, 215–228.

Huerre, P. & Monkewitz, P. A. 1985 Absolute and convective instabilities in free shear layers. *J. Fluid Mech.* **159**, 151–168.

Huerre, P. & Monkewitz, P. A. 1990 Local and global instabilities in spatially developing flows. *Annu. Rev. Fluid Mech.* **22**, 473–537.

Jendoubi, S. & Strykowski, P. J. 1994 Absolute and convective instability of axisymmetric jets with external flow. *Phys. Fluids* **6**, 3000–3009.

Kambe, T. 1969 The stability of an axisymmetric jet with parabolic profile. *J. Phys. Soc. Jpn.* **26** (2), 566–575.

Kelvin, Lord 1871 Hydrokinetic solutions and observations. *Phil Mag. (4)* **42**, 362–377.

Kyle, D. M. & Sreenivasan, K. R. 1993 The instability and breakdown of a round variable-density jet. *J. Fluid Mech.* **249**, 619–664.

Landau, L. & Lifschitz, E. M. 1954 *Mechanics of Continuous Media*. Moscow: Fizmatgiz (In Russian).

Lessen, M. & Singh, P. J. 1973 The stability of axisymmetric free shear layers. *J. Fluid Mech.* **60** (3), 433–457.

Lesshafft, L. & Huerre, P. 2007 Linear impulse response in hot round jets. *Phys. Fluids* **19** (2), 024102.

Lesshafft, L., Huerre, P., Sagaut, P. & Terracol, M. 2006 Nonlinear global modes in hot jets. *J. Fluid Mech.* **554**, 393–409.

Mattingly, G. E. & Chang, C. C. 1974 Unstable waves on an axisymmetric jet column. *J. Fluid Mech.* **65** (3), 541–560.

Mollendorf, J. C. & Gebhart, B. 1973 An experimental and numerical study of the viscous stability of a round laminar vertical jet with and without thermal buoyancy for symmetric and asymmetric disturbances. *J. Fluid Mech.* **61** (2), 367–399.

Monkewitz, P. A. 1988 The absolute and convective nature of instability in two-dimensional wakes at low reynolds numbers. *Phys. Fluids* **31**, 999–1006.

Monkewitz, P. A., Bechert, D. W., Barsikow, B. & Lehmann, B. 1990 Self-excited oscillations and mixing in a heated round jet. *J. Fluid Mech.* **213**, 611–639.

Monkewitz, P. A., Lehmann, B., Barsikow, B. & Bechert, D. W. 1989 The spreading of self-excited hot jets by side jets. *Phys. Fluids A* **1** (3), 446–448.

Morris, P. J. 1976 The spatial viscous instability of axisymmetric jets. *J. Fluid Mech.* **77** (3), 511–529.

Nichols, J. W., Schmid, P. J. & Riley, J. J. 2007 Self-sustained oscillations in variable-density round jets. *J. Fluid Mech.* **582**, 341–376.

Raghu, S. & Monkewitz, P. A. 1991 The bifurcation of a hot round jet to limit-cycle oscillations. *Phys. Fluids* **3** (4), 501–503.

Rayleigh, Lord 1880 On the stability, or instability, of certain fluid motions. *Proc. London Math. Soc.* **11**, 57–70.

Reynolds, A. J. 1962 Observations of a liquid-into-liquid jet. *J. Fluid Mech.* **14**, 552–556.

Sevilla, A., Gordillo, J. M. & Martínez-Bazán, C. 2002 The effect of the diameter ratio on the absolute and convective instability of free coflowing jets. *Phys. Fluids* **14**, 3028–3038.

Sreenivasan, K. R., Raghu, S. & Kyle, D. 1989 Absolute instability in variable density round jets. *Exps. Fluids* **7**, 309–317.

Srinivasan, K., Hallberg, M. P. & Strykowski, P. J. 2010 Viscous linear stability of axisymmetric low-density jets: Parameters influencing absolute instability. *Phys. Fluids* **22**, 024103.

Sturrock, P. A. 1958 Kinematics of growing waves. *Phys. Rev.* **112**, 1488–1503.

Tam, C. K. W. 1971 Directional acoustic radiation from a supersonic jet generated by shear layer isntability. *J. Fluid Mechanics* **46**, 757–768.

Twiss, Q. 1951 On oscillations in electron streams. *Proc. Phys. Soc. (London)* **B64**, 654–669.

Twiss, Q. 1952 Propagation in electron-ion streams. *Phys. Rev.* **88**, 1392–1407.

Yu, M.-H. & Monkewitz, P. A. 1990 The effect of nonuniform density on the absolute instability of two-dimensional inertial wakes and jets. *Phys. Fluids A* **2**, 611–639.

CHAPTER

TWO

Theoretical background

2.1 Base flow

The flow considered in the present work is that of a hot jet emerging from a round injector discharging into a cooler stagnant atmosphere. The properties of the jet are denoted with the subscript $_j$ whereas the properties of the atmosphere far from the injector are denoted with the subscript $_\infty$. Therefore, the density and viscosity at the injector exit are ρ_j, μ_j whereas the density and viscosity of the atmosphere are ρ_∞, μ_∞. A schematic of the flow configuration can be seen in figure 2.1. The injector is a straight round tube of length l_t and constant radius a. The flow rate is Q and the flow enters the injector with uniform velocity $u_j = \frac{Q}{\pi a^2}$. The Reynolds number based on this velocity, $Re = \frac{\rho_j u_j a}{\mu_j}$, is assumed to be high. This results into a slender jet with a characteristic length of the jet flow of $Re\, a \gg 1$. Buoyancy effects have been neglected as the Richardson number $Ri = (\rho_\infty - \rho_j)ga/(\rho_j u_j^2) \ll 1$.

The stability characteristics of the flow in slender low-density jets have been proven to be very sensitive to the initial velocity profile at the injector exit. In order to obtain realistic velocity profiles the flow field inside the injector tube is computed numerically from the dimensionless continuity and momentum equations in the boundary-layer approximation since $Re \gg 1$. The equations are nondimensionalized rescaling r^*,x^*,u^* and v^* with a,$Re\, a$, u_j and $\frac{\mu_j}{\rho_j a}$, respectively. The * denotes a dimensional variable. The density is assumed to be constant along the injector tube as the injector walls are considered adiabatic and the Mach number $Ma = \frac{u_j}{c_0}$ is small, with c_0 representing the speed of sound in the fluid.

The boundary layer approximation is based on the assumption that the axial development of the flow, of the order of L, is much greater than its radial development, of order δ. Therefore, if $u \sim u_j$, v, from continuity, is $v \sim (\delta/L)u_j$. That way $u\frac{\partial v}{\partial x} \sim v\frac{\partial u}{\partial r} \ll u\frac{\partial u}{\partial x} \sim v\frac{\partial u}{\partial r}$, $\frac{\partial^2 v}{\partial x^2} \ll \frac{\partial^2 u}{\partial x^2} \ll \frac{\partial^2 v}{\partial r^2} \ll \frac{\partial^2 u}{\partial r^2}$ and $\frac{\partial p}{\partial r} \sim 0$.

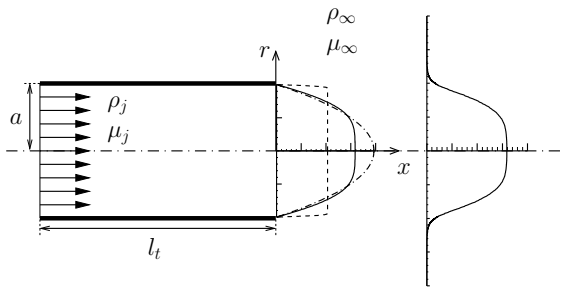

Figure 2.1: Schematic of the flow configuration. Figure taken from Coenen (2010)

Therefore, the continuity and momentum equations in the boundary layer approximation for the flow inside the injector tube are

$$\frac{\partial(ru)}{\partial x} + \frac{\partial(rv)}{\partial r} = 0, \tag{2.1a}$$

$$u\frac{\partial u}{\partial x} + v\frac{\partial u}{\partial r} = -P_l + \frac{1}{r}\frac{\partial}{\partial r}(r\frac{\partial u}{\partial r}), \tag{2.1b}$$

which are integrated numerically using the method of lines (Holmes (2007)) with initial conditions $u = 1$ at $x = -L_t$ and boundary conditions $\frac{\partial u}{\partial r} = v = 0$ at $r = 0$ and $u = v = 0$ at $r = 1$ for $x > -L_t$. Where $L_t = \frac{l_t}{Re_a}$ is the rescaled injector length and P_l a rescaled axial pressure gradient. In this manner we obtain the velocity profile at the injector exit that will be the initial conditions for the jet flow.

In order to obtain the steady solution for the flow field in the downstream of the injector exit, the axisymmetric dimensionless boundary-layer equations are used. In this case, given that the variations of pressure radially are very small according to the boundary layer approximation $\frac{\partial p}{\partial r} \ll 1$, and the fact that when $r \to \infty$ the flow is at rest and thus the pressure is the same independently of x, the axial variations of pressure $\frac{\partial p}{\partial x} = 0$. Therefore, the equations of motion for the flow downstream of the injector exit are the continuity and momentum equations,

$$\frac{\partial}{\partial x}(\rho ru) + \frac{\partial}{\partial r}(\rho rv) = 0, \tag{2.2a}$$

$$\rho(u\frac{\partial u}{\partial x} + v\frac{\partial u}{\partial r}) = \frac{1}{r}\frac{\partial}{\partial r}(\mu r\frac{\partial u}{\partial r}), \tag{2.2b}$$

and the energy equation approximated for low Mach numbers

$$\rho(u\frac{\partial T}{\partial x} + v\frac{\partial T}{\partial r}) = \frac{1}{Pr}\frac{1}{r}\frac{\partial}{\partial r}(\mu r\frac{\partial T}{\partial r}), \tag{2.2c}$$

where u, μ, T, κ are nondimensionalized with $u_j, \mu_j, T_j, \kappa_j$ The initial conditions to integrate these equations are $u = u_e(r), T = 1$ for $r \leq 1$ and $u = 0, T = S$ for $r > 1$ at $x = 0$, and the boundary conditions are $\frac{\partial u}{\partial r} = v = \frac{\partial T}{\partial r} = 0$ at $r = 0$ and $u = v = 0, T = S$ as $r \to \infty$ for $x > 0$.

The equation of state written in the quasi-isobaric approximation

$$\rho T = 1 \tag{2.3a}$$

and the presumed power-law temperature dependence

$$\mu = \kappa = T^{\sigma} \tag{2.3b}$$

supplement the conservation equations for the transport properties. For equation 2.3b it is assumed that the Prandtl number Pr and the specific heat at constant pressure c_p^* remain constant along the flow ($\mu = \kappa$).

These equations are integrated numerically using a finite differences approach with a second-order scheme in r and starting at $x = 0$ and then marching in $x > 0$. The numerical integration is explained in more detail in appendix A.

2.2 Stability analysis

The linear stability analysis performed here is based on the addition of small perturbations to the base flow and analyzing the spatiotemporal response of the flow to those perturbations. Azimuthal perturbations where not included in the analysis as it has been observed that for this kind of flows the axisymmetric mode is dominant under most conditions (see for instance Monkewitz *et al.* (1990)). The dimensionless equations of motion describing the stability problem are

$$\frac{\partial \rho}{\partial t} + \nabla \cdot (\rho \mathbf{u}) = 0 \tag{2.4a}$$

$$\rho\left(\frac{\partial \mathbf{u}}{\partial t} + \mathbf{u} \cdot \nabla \mathbf{u}\right) = -\nabla p + \frac{1}{Re}\left\{\nabla \cdot [\mu(\nabla \mathbf{u} + \nabla \mathbf{u}^T)] - \frac{2}{3}\nabla(\mu \nabla \cdot \mathbf{u})\right\} \tag{2.4b}$$

$$\rho\left(\frac{\partial T}{\partial t} + \mathbf{u} \cdot \nabla T\right) = \frac{1}{RePr}\nabla \cdot (\kappa \nabla T) \tag{2.4c}$$

However, in contrast to the base flow analysis, the axial coordinate x^* is nondimensionalized with the jet radius a as the characteristic length scale. Also, time t is scaled with a/u_j.

Perturbations of the basic flow are inserted in the equations of motion as follows:

$$
\begin{aligned}
u &= \bar{u} + \tilde{u}, & v &= \bar{v} + \tilde{u}, \\
\rho &= \bar{\rho} + \tilde{\rho}, & T &= \bar{T} + \tilde{T}, \\
\mu &= \bar{\mu} + \tilde{\mu}, & \kappa &= \bar{\kappa} + \tilde{\kappa}, \\
p &= \tilde{p}, &
\end{aligned}
$$

where $\bar{u}, \bar{v}, \bar{\rho}, ...$ represent the base flow values and $\hat{u}, \hat{v}, \hat{\rho}, ...$ represent the perturbations. In the subsequent substitution, the terms containing only base flow quantities satisfy the steady equations of motion and can therefore be removed from the development. With the rest of the terms, a linearization is performed. The perturbations are assumed to be small, of order $\epsilon \ll 1$. Therefore, the terms containing products of perturbations are of order ϵ^2 and are neglected.

We will now perform an analysis of the order of magnitude of the terms that remain. The characteristic axial length of the base flow is $Re\,a$ while the characteristic length for the stability analysis is a. This results in $x \sim O(Re)$ for the base flow while $x \sim O(1)$ for the stability flow. The orders of magnitude of the properties of the perturbations and the base flow are

$$
\begin{aligned}
&(\rho, u, v, p, \mu, T, \frac{\partial \rho}{\partial x}, \frac{\partial u}{\partial x}, \frac{\partial v}{\partial x}, \frac{\partial p}{\partial x}, \frac{\partial \mu}{\partial x}, \frac{\partial T}{\partial x}, \\
&\rho', u', v', p', \mu', T', \frac{\partial^2 u}{\partial x^2}, u'', \frac{\partial^2 v}{\partial x^2}, v'') && \sim && O(\epsilon), \\
&(\bar{\rho}, \bar{u}, \bar{\mu}, \bar{T}, \bar{\rho}', \bar{u}', \bar{\mu}', \bar{T}') && \sim && O(1), \\
&(\bar{v}, \bar{v}', \bar{v}'', \frac{\partial \bar{\rho}}{\partial x}, \frac{\partial \bar{u}}{\partial x}, \frac{\partial \bar{\mu}}{\partial x}, \frac{\partial \bar{T}}{\partial x}) && \sim && O(1/Re), \\
&(\frac{\partial \bar{v}}{\partial x}, \frac{\partial^2 \bar{u}}{\partial x^2}, \frac{\partial^2 \bar{T}}{\partial x^2}) && \sim && O(1/Re^2),
\end{aligned}
$$

where the tilde has been omitted here and onwards to denote the perturbations and the $'$,$''$ denote the partial derivatives with respect to r $\frac{\partial}{\partial r}, \frac{\partial^2}{\partial r^2}$. Next, an analysis of the orders of magnitude for each of the terms in the conservation equations is shown, where terms of O(ϵ/Re) containing base flow non-parallelism have been highlighted in bold,

Continuity:

$$\underbrace{\frac{\partial \rho}{\partial t}}_{O(\epsilon)} + \underbrace{\frac{\partial \bar{\rho}}{\partial x} u}_{\boldsymbol{O(\epsilon/Re)}} + \underbrace{\bar{\rho}\frac{\partial u}{\partial x}}_{O(\epsilon)} + \underbrace{\frac{\partial \rho}{\partial x}\bar{u}}_{O(\epsilon)} + \underbrace{\rho\frac{\partial \bar{u}}{\partial x}}_{\boldsymbol{O(\epsilon/Re)}} + \underbrace{\bar{\rho}\frac{v}{r}}_{O(\epsilon)} +$$
$$+ \underbrace{\bar{\rho}' v}_{O(\epsilon)} + \underbrace{\bar{\rho} v'}_{O(\epsilon)} + \underbrace{\rho\frac{\bar{v}}{r}}_{\boldsymbol{O(\epsilon/Re)}} + \underbrace{\rho' \bar{v}}_{\boldsymbol{O(\epsilon/Re)}} + \underbrace{\rho \bar{v}'}_{\boldsymbol{O(\epsilon/Re)}} = 0. \tag{2.5a}$$

Axial momentum:

$$\underbrace{\bar{\rho}\frac{\partial u}{\partial t}}_{O(\epsilon)} + \underbrace{\bar{\rho}\bar{v}u'}_{\boldsymbol{O(\epsilon/Re)}} + \underbrace{\bar{\rho} v \bar{u}'}_{O(\epsilon)} + \underbrace{\bar{\rho}\bar{u}\frac{\partial u}{\partial x}}_{O(\epsilon)} + \underbrace{\bar{\rho} u \frac{\partial \bar{u}}{\partial x}}_{\boldsymbol{O(\epsilon/Re)}} + \underbrace{\rho \bar{v}\bar{u}'}_{\boldsymbol{O(\epsilon/Re)}} + \underbrace{\rho \bar{u}\frac{\partial \bar{u}}{\partial x}}_{\boldsymbol{O(\epsilon/Re)}} =$$
$$\underbrace{-\frac{\partial p}{\partial x}}_{O(\epsilon)} + \frac{1}{Re}\Big(\underbrace{\bar{\mu}\nabla^2 u}_{O(\epsilon/Re)} + \underbrace{\mu\frac{\partial^2 \bar{u}}{\partial x^2}}_{O(\epsilon/Re^3)} + \underbrace{\mu\frac{1}{r}(r\bar{u}')'}_{O(\epsilon/Re)} + \underbrace{\frac{1}{3}\bar{\mu}\frac{\partial(\nabla\cdot\mathbf{u})}{\partial x}}_{O(\epsilon/Re)} + \underbrace{\frac{1}{3}\mu\frac{\partial(\nabla\cdot\bar{\boldsymbol{u}})}{\partial x}}_{O(\epsilon/Re^2)} +$$
$$+ \underbrace{\mu'\bar{u}'}_{O(\epsilon/Re)} + \underbrace{2\frac{\partial \mu}{\partial x}\frac{\partial \bar{u}}{\partial x}}_{O(\epsilon/Re^2)} + \underbrace{\bar{\mu}'\frac{\partial v}{\partial x}}_{O(\epsilon/Re)} + \underbrace{\bar{\mu}' u'}_{O(\epsilon/Re)} + \underbrace{2\frac{\partial \bar{\mu}}{\partial x}\frac{\partial u}{\partial x}}_{O(\epsilon/Re^2)} - \underbrace{\frac{2}{3}\frac{\partial \mu}{\partial x}\nabla\cdot\bar{\boldsymbol{u}}}_{O(\epsilon/Re^2)}\Big). \tag{2.5b}$$

Radial momentum:

$$\underbrace{\bar{\rho}\frac{\partial v}{\partial t}}_{O(\epsilon)} + \underbrace{\bar{\rho}\bar{v}v'}_{\boldsymbol{O(\epsilon/Re)}} + \underbrace{\bar{\rho} v \bar{v}'}_{\boldsymbol{O(\epsilon/Re)}} + \underbrace{\bar{\rho}\bar{u}\frac{\partial v}{\partial x}}_{O(\epsilon)} + \underbrace{\bar{\rho} u \frac{\partial \bar{v}}{\partial x}}_{O(\epsilon/Re^2)} + \underbrace{\rho \bar{v}\bar{v}'}_{O(\epsilon/Re^2)} + \underbrace{\rho \bar{u}\frac{\partial \bar{v}}{\partial x}}_{O(\epsilon/Re^2)} =$$
$$\underbrace{-p'}_{O(\epsilon)} + \frac{1}{Re}\Big(\underbrace{\bar{\mu}\nabla^2 v}_{O(\epsilon/Re)} - \underbrace{\bar{\mu}\frac{v}{r^2}}_{O(\epsilon/Re)} + \underbrace{\mu\frac{1}{r}(r\bar{v}')'}_{O(\epsilon/Re^2)} + \underbrace{\frac{1}{3}\bar{\mu}(\nabla\cdot\mathbf{u})'}_{O(\epsilon/Re)} + \underbrace{\frac{1}{3}\mu(\nabla\cdot\bar{\boldsymbol{u}})'}_{O(\epsilon/Re^2)} +$$
$$+ \underbrace{2\mu'\bar{v}'}_{O(\epsilon/Re^2)} + \underbrace{\frac{\partial \mu}{\partial x}\bar{u}'}_{O(\epsilon/Re)} + \underbrace{\bar{\mu}'(2v' - \frac{2}{3}\nabla\cdot\mathbf{u})}_{O(\epsilon/Re)} + \underbrace{(\frac{\partial v}{\partial x} + u')\frac{\partial \bar{\mu}}{\partial x}}_{O(\epsilon/Re^2)} - \underbrace{\frac{2}{3}\mu'\nabla\cdot\bar{\boldsymbol{u}}}_{O(\epsilon/Re^2)}\Big). \tag{2.5c}$$

Energy:

$$\underbrace{\bar{\rho}\frac{\partial T}{\partial t}}_{O(\epsilon)} + \underbrace{\bar{\rho}\bar{u}\frac{\partial T}{\partial x}}_{O(\epsilon)} + \underbrace{\bar{\rho}\bar{v}T'}_{\boldsymbol{O(\epsilon/Re)}} + \underbrace{\bar{\rho}u\frac{\partial \bar{T}}{\partial x}}_{\boldsymbol{O(\epsilon/Re)}} + \underbrace{\bar{\rho}v\bar{T}'}_{O(\epsilon)} + \underbrace{\rho\bar{u}\frac{\partial \bar{T}}{\partial x}}_{\boldsymbol{O(\epsilon/Re)}} +$$
$$+ \underbrace{\rho\bar{v}\bar{T}'}_{\boldsymbol{O(\epsilon/Re)}} = \frac{1}{RePr}(\underbrace{\bar{\kappa}\nabla^2 T}_{O(\epsilon/Re)} + \underbrace{\frac{\partial\bar{\kappa}}{\partial x}\frac{\partial T}{\partial x}}_{O(\epsilon/Re^2)} + \underbrace{\bar{\kappa}'T'}_{O(\epsilon/Re)} + \underbrace{\kappa\frac{\partial^2\bar{T}}{\partial x^2}}_{O(\epsilon/Re^3)} +$$
$$+ \underbrace{\kappa\bar{T}''}_{O(\epsilon/Re)} + \underbrace{\frac{\kappa}{r}\bar{T}'}_{O(\epsilon/Re)} + \underbrace{\kappa'\bar{T}'}_{O(\epsilon/Re)} + \underbrace{\frac{\partial\kappa}{\partial x}\frac{\partial\bar{T}}{\partial x}}_{O(\epsilon/Re^2)}). \tag{2.5d}$$

As $Re \gg 1$, terms of order (ϵ/Re^2) are considered negligible. However, terms of order $O(1/Re)$ remain significant. In those terms of order $O(1/Re)$ is where the present work is different from what has been done up to now. When performing linear stability analysis of slender low density jets, non-parallel terms of the base flow $(\bar{v}, \frac{\partial\bar{\phi}}{\partial x})$ are discarded because they are considered negligible $(O(1/Re))$ compared to the parallel base flow terms $(O(1))$. However, it is perfectly valid to retain them in the analysis. When the perturbations are inserted into the equations of motion, it can be seen that there are terms containing non-parallelism of the base flow that are of the same order as other terms that contain only strictly parallel base flow properties. Those non-parallel terms of order $O(\epsilon/Re)$ can be seen in equations 2.5a,2.5b,2.5c and 2.5d highlighted in bold.

If we keep those non-parallel terms of the same order of magnitude that we were already keeping with the parallel ones $(O(1/Re))$, the linearized equations of motion take the form:

$$\frac{\partial\rho}{\partial t} + \underbrace{\frac{\partial\bar{\rho}}{\partial x}u}_{n.p} + \bar{\rho}\frac{\partial u}{\partial x} + \frac{\partial\rho}{\partial x}\bar{u} + \underbrace{\rho\frac{\partial\bar{u}}{\partial x}}_{n.p} + \bar{\rho}\frac{v}{r} + \bar{\rho}'v + \bar{\rho}v' + \underbrace{\rho\frac{\bar{v}}{r} + \rho'\bar{v} + \rho\bar{v}'}_{n.p} = 0, \tag{2.6a}$$

$$\bar{\rho}\frac{\partial u}{\partial t} + \underbrace{\bar{\rho}\bar{v}u'}_{n.p} + \bar{\rho}v\bar{u}' + \bar{\rho}\bar{u}\frac{\partial u}{\partial x} + \underbrace{\bar{\rho}u\frac{\partial\bar{u}}{\partial x} + \rho\bar{v}\bar{u}' + \rho\bar{u}\frac{\partial\bar{u}}{\partial x}}_{n.p} = -\frac{\partial p}{\partial x} +$$
$$\frac{1}{Re}(\bar{\mu}\nabla^2 u + \mu\bar{u}'' + \frac{\mu}{r}\bar{u}' + \frac{1}{3}\bar{\mu}\frac{\partial(\nabla\cdot\mathbf{u})}{\partial x} + \mu'\bar{u}' + \bar{\mu}'\frac{\partial v}{\partial x} + \bar{\mu}'u'), \tag{2.6b}$$
$$\bar{\rho}\frac{\partial v}{\partial t} + \underbrace{\bar{\rho}\bar{v}v' + \bar{\rho}v\bar{v}'}_{n.p} + \bar{\rho}\bar{u}\frac{\partial v}{\partial x} = -\frac{\partial p}{\partial r} + \frac{1}{Re}(\bar{\mu}\nabla^2 v - \bar{\mu}\frac{v}{r^2} +$$

$$+\frac{1}{3}\bar{\mu}\frac{\partial(\nabla\cdot\mathbf{u})}{\partial r}+\frac{\partial\mu}{\partial x}\bar{u}'+\bar{\mu}'(2v'-\frac{2}{3}\nabla\cdot\mathbf{u})), \tag{2.6c}$$

$$\bar{\rho}\frac{\partial T}{\partial t}+\bar{\rho}\bar{u}\frac{\partial T}{\partial x}+\underbrace{\bar{\rho}\bar{v}T'+\bar{\rho}u\frac{\partial\bar{T}}{\partial x}}_{n.p}+\bar{\rho}v\bar{T}'+\underbrace{\rho\bar{u}\frac{\partial\bar{T}}{\partial x}+\rho\bar{v}\bar{T}'}_{n.p}=$$

$$\frac{1}{RePr}(\bar{\kappa}\nabla^2T+\bar{\kappa}'T'+\kappa\bar{T}''+\frac{\kappa}{r}\bar{T}'+\kappa'\bar{T}'), \tag{2.6d}$$

where non parallel terms have been underlined for an easier identification.

Next, the perturbations are assumed to be normal modes,

$$(\rho,T,\mu,\kappa,u,v,p)=(\hat{\rho},\hat{T},\hat{\mu},\hat{\kappa},\hat{u},i\hat{v},\hat{p})e^{i(kx-\omega t)} \tag{2.7}$$

where k and ω are complex numbers.

Inserting the shape of the perturbations into the linearized equations of motion (2.5a-2.5d) we obtain:

$$(k\bar{u}-\underbrace{i(\frac{\bar{v}}{r}+\bar{v}'+\frac{\partial\bar{u}}{\partial x}))\hat{\rho}-i\bar{v}\hat{\rho}'}_{n.p}+(k\bar{\rho}-\underbrace{i\frac{\partial\bar{\rho}}{\partial x}}_{n.p})\hat{u}+(\frac{\bar{\rho}}{r}+\bar{\rho}')\hat{v}+\bar{\rho}\hat{v}'=\omega\hat{\rho}, \tag{2.8a}$$

$$-\underbrace{(\bar{v}\bar{u}'+\bar{u}\frac{\partial\bar{u}}{\partial x})\hat{\rho}}_{n.p}+\frac{1}{Re}(\bar{u}''+\frac{\bar{u}'}{r})\hat{\mu}+\frac{1}{Re}(\bar{u}')\hat{\mu}'-(ik\bar{\rho}\bar{u}+\underbrace{\bar{\rho}\frac{\partial\bar{u}}{\partial x}}_{n.p}+$$

$$+\frac{4}{3Re}k^2\bar{\mu})\hat{u}+(\underbrace{-\bar{\rho}\bar{v}}_{n.p}+\frac{1}{Re}(\frac{\bar{\mu}}{r}+\bar{\mu}'))\hat{u}'+\frac{1}{Re}(\bar{\mu})\hat{u}''+(-i\bar{\rho}\bar{u}'+$$

$$-\frac{1}{Re}(\frac{1}{3}\frac{k\bar{\mu}}{r}+k\bar{\mu}'))\hat{v}-\frac{1}{3}k\bar{\mu}\hat{v}'+-ik\hat{p}=-i\omega\bar{\rho}\hat{u}, \tag{2.8b}$$

$$-\frac{1}{Re}k\bar{u}'\hat{\mu}+\frac{2}{3Re}k\bar{\mu}'\hat{u}-\frac{1}{3Re}\bar{\mu}k\hat{u}'+(\underbrace{\bar{\rho}\bar{v}'}_{n.p}+ik\bar{\rho}\bar{u}+$$

$$+\frac{1}{Re}(k^2\bar{\mu}+\frac{4}{3r^2}\bar{\mu}+\frac{2}{3r}\bar{\mu}'))\hat{v}+(\underbrace{\bar{\rho}\bar{v}}_{n.p}-\frac{1}{Re}(\frac{4}{3r}\bar{\mu}+\frac{4}{3}\bar{\mu}'))\hat{v}'$$

$$-\frac{4}{3Re}\bar{\mu}\hat{v}''-i\hat{p}'=i\bar{\rho}\omega\hat{v}, \tag{2.8c}$$

$$\underbrace{(\bar{u}\frac{\partial\bar{T}}{\partial x}+\bar{v}\bar{T}')\hat{\rho}}_{n.p}-(\frac{\bar{T}'}{r}\bar{T}'+\bar{T}'')\hat{\kappa}-\bar{T}'\hat{\kappa}'+(ik\bar{\rho}\bar{u}+\frac{k^2\bar{\kappa}}{RePr})\hat{T}+$$

$$+(\underbrace{\bar{\rho}\bar{v}}_{n.p}-\frac{\frac{\bar{\kappa}}{r}+\bar{\kappa}'}{RePr})\hat{T}'+(\bar{\kappa})\hat{T}''+\underbrace{\bar{\rho}\frac{\partial\bar{T}}{\partial x}\hat{u}}_{n.p}+i\bar{\rho}\bar{T}'\hat{v}=i\omega\bar{\rho}\hat{T}, \tag{2.8d}$$

The boundary conditions of those stability equations far from the injector exit is that the perturbations die out

$$r\to\infty: \quad (\hat{\rho},\hat{T},\hat{\mu},\hat{\kappa},\hat{u},\hat{v},\hat{p})\to 0. \tag{2.9}$$

At the other end, at $r=0$ the boundary conditions are that there is no radial velocity of the perturbation $\hat{v}=0$, $\hat{u}'=0$ and $\hat{u},\hat{\rho},\hat{\mu},\hat{\kappa},\hat{T},\hat{p}$ values must be finite.

$$r=0: \quad \hat{v}=\hat{u}'=0 \quad \text{and} \quad (\hat{\rho},\hat{T},\hat{\mu},\hat{\kappa},\hat{p}) \text{ finite.} \tag{2.10}$$

A Taylor expansion of equations 2.8b, 2.8cand 2.8d around $r=0$ yields

$$r=0: \begin{cases} \hat{\mu}\bar{u}'+\bar{\mu}\hat{u}'=0 \\ -\frac{2}{3}k(\bar{\mu}\hat{u}'+\bar{\mu}'\hat{u})+(\frac{2}{3}\bar{\mu}'-\underbrace{Re\bar{\rho}\bar{v}}_{n.p})\hat{v}'+2\bar{\mu}\hat{v}''+iRe\hat{p}'=0 \\ \bar{T}'\hat{\kappa}+\hat{T}'\bar{\kappa}=0 \end{cases} \tag{2.11}$$

The set of stability equations result into an eigenvalue problem at each streamwise location of the form $\boldsymbol{A}(k)\boldsymbol{x}=\omega\boldsymbol{B}\boldsymbol{x}$ where $\boldsymbol{A}$ and $\boldsymbol{B}$ are matrices and $\boldsymbol{x}$ is the vector $\boldsymbol{x}=[\hat{\rho}\ \hat{u}\ \hat{v}\ \hat{p}]'$ containing the set of eigenfunctions $\psi(r)$=$(\hat{\rho},\hat{u},\hat{v},\hat{p})$(r). These eigenfunctions only exist if k and ω satisfy a dispersion relation

$$D[k,\omega;R]=0 \tag{2.12}$$

where R represents all those parameters that determine the base flow characteristics Re,Pr,S, etc. The dispersion relation is the spectral form of the differential operator in physical space $D[-i\frac{\partial}{\partial x},i\frac{\partial}{\partial t};R]$ coming from the equations of motion so that perturbations $\psi(x,t)$ conform to

$$D(-i\frac{\partial}{\partial x},i\frac{\partial}{\partial t};R)\psi(x,t)=0.$$

2.2.1 Linear local hydrodynamic stability theory

There are some key stability concepts. The terms local and global refer to the stability conditions at one specific streamwise location or to the stability of the entire flow respectively. When localized perturbations grow in time but are

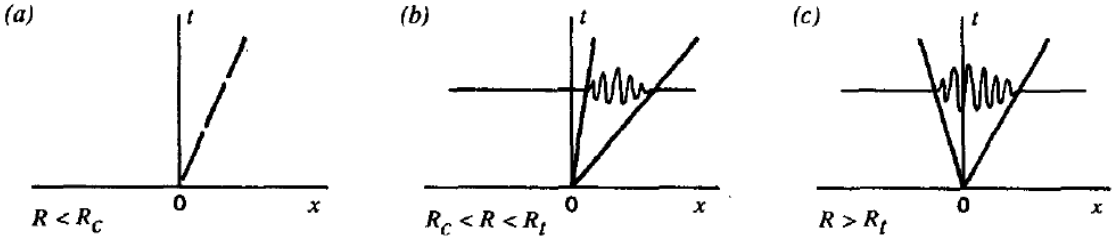

Figure 2.2: Typical impulse responses. (a) stable, (b) convectively unstable, (c) absolutely unstable. Figure taken from Huerre & Monkewitz (1990).

washed away downstream the base flow is said to be locally convectively unstable (Figure 2.2b), whereas when disturbances grow in time but travel both downstream and upstream the base flow is said to be locally absolutely unstable (Figure 2.2c).

In order to study the absolute or convective nature of the local instabilities, we are interested in the modes with zero group velocity (k_0, ω_0 so that $d\omega(k)/dk = 0$), which physically means we want to analyze the behavior of those wave packets that remain at the source, amplifying or decaying. Graphically this means the study of the line $x/t = 0$ in figure 2.2. From the modes with zero group velocity we can tell, depending on whether the perturbations asymptotically ($t \to \infty$) amplify or attenuate at the source, the absolute or convective nature of the local instability from the value of the absolute growth rate $\omega_{0,i}$. If $\omega_{0,i} > 0$ the flow is locally absolutely unstable whereas if $\omega_{0,i} < 0$ the flow is locally convectively unstable. To compute the value of $\omega_{0,i}$ at each streamwise location, we make use of the fact that the condition for the existence of wave packets of zero velocity, $d\omega(k_0)/dk = 0$, implies the existence of a saddle point in the complex solution space for (k, ω). From all existing saddle points, the one with the largest $\omega_{0,i}$, while satisfying the Briggs-Bers criterion (Briggs (1964)), is the one that determines the asymptotic ($t \to \infty$) response to an instantaneous impulse of the flow at that location. The numerical method used to compute the value of $\omega_{0,i}$ can be found in the appendix A.

2.2.2 Global stability criteria

Given the evolution of local stability properties, specifically the absolute growth rate, $\omega_{0,i}$, in the streamwise direction, the global stability properties of the flow can be inferred from it. Depending on the shape of that evolution we can distinguish four different cases. Those four different cases are shown in figure 2.3. In case I, the value of $\omega_{0,i}$ is smaller than 0 for every streamwise location x. This means that the flow is convectively unstable. In case II however, there is

a pocket of local absolute instability, where $\omega_{0,i}$ is greater than 0. In this case the pocket of local absolute instability would contaminate the entire flow so that globally the flow would be absolutely unstable. This will happen independently of the size of the locally unstable region (Pier *et al.* (1998);Lesshafft *et al.* (2006);Sevilla (2011)). Whenever that pocket of local absolute instability reaches the upstream boundary of the flow we can differentiate between two cases. In case III, the derivative of the absolute growth rate at the injector outlet $\frac{\partial}{\partial x}(\omega_{0,i}(0))$ is positive. The flow is considered absolutely unstable in this case as this type of evolution is assumed equivalent to case II. In case IV however, where the pocket of local absolute instability reaches the upstream boundary of the flow and $\frac{\partial}{\partial x}(\omega_{0,i}(0)) < 0$, additional information is needed to be able to determine which are the global stability properties of the flow. For this type of evolution of the absolute growth rate, the pocket of local absolute instability of length x_{AC} would need to be big enough in order to trigger global absolute instability (Chomaz *et al.* (1988);Couairon & Chomaz (1999)). If the pocket of absolute instability were smaller than a certain critical length l_c, the flow would remain globally convectively unstable due to the stabilizing effect of the convection in the region near the injector exit. Whereas if that region of local absolute instability were greater than that critical value l_c, the flow would be globally unstable.

There are various options for defining that critical length l_c mentioned before, past which the region of absolute instability bounded by the injector outlet would contaminate the whole flow making it absolutely unstable. However, none of them have been found to be completely satisfactory. One option is based on the numerical results of Lesshafft *et al.* (2006). They found that global absolute instability was triggered when the locally absolutely unstable region reached a length of the order of the absolute wavelength of the instability at the injector outlet. Therefore one criteria would consist in setting $l_c = \lambda(0) = 2\pi/k_{0,r}(0)$. However, this criteria has some uncertainty associated to it as it is based on numerical evidence and not on solid theoretical principles. Another criterion (Chomaz *et al.* (1988)), theoretically more sound but developed for the Ginzburg-Landau equation and not the Navier-Stokes equations, consist on setting the critical length to $l_c = C/\sigma_0^{-1/2}$ were σ_0 corresponds to the absolute growth rate at the injector outlet $\omega_{0,i}(0)$ and C is a constant. The problem with this criteria is the need to adjust for the constant C based on previous experimental results.

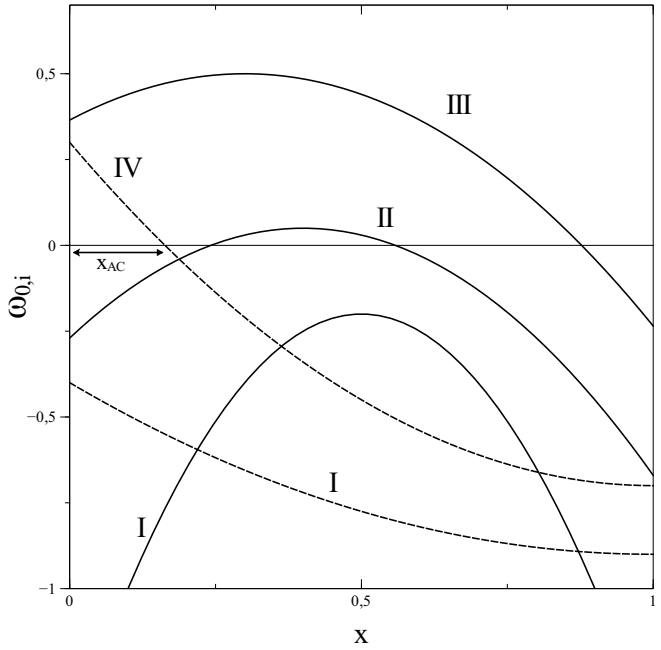

Figure 2.3: Types of streamwise evolutions of $\omega_{0,i}$ determining the globally convective or absolute nature of the instability of the flow: (I) convectively unstable, (II) absolutely unstable, (III) absolutely unstable, (IV) absolutely unstable or convectively unstable depending on whether the length x_{AC} is greater or lower than a critical value l_c. Solid lines represent streamwise evolutions of $\omega_{0,i}$ where $d\omega_{0,i}/dx(x = 0) > 0$ whereas dashed lines correspond to those where $d\omega_{0,i}/dx(x = 0) < 0$.

References

Briggs, R. J. 1964 *Electron-stream interaction with plasmas (Research monograph no. 29)*. MIT Press.

Chomaz, J. M., Huerre, P. & Redekopp, L. G. 1988 Bifurcation to local and global modes in spatially developing flows. *Phys. Rev. Lett.* **60**, 25–.

Coenen, W. 2010 Absolute instability in the near field of low-density jets. PhD thesis, Universidad Carlos III de Madrid.

Couairon, A & Chomaz, J. M. 1999 Fully nonlinear global modes in slowly varying flows. *Phys. Fluids* **11**, 3688–3703.

Holmes, M. H. 2007 *Introduction to Numerical Methods in Differential Equations*. Springer, New York.

Huerre, P. & Monkewitz, P. A. 1990 Local and global instabilities in spatially developing flows. *Annu. Rev. Fluid Mech.* **22**, 473–537.

Lesshafft, L., Huerre, P., Sagaut, P. & Terracol, M. 2006 Nonlinear global modes in hot jets. *J. Fluid Mech.* **554**, 393–409.

Monkewitz, P. A., Bechert, D. W., Barsikow, B. & Lehmann, B. 1990 Self-excited oscillations and mixing in a heated round jet. *J. Fluid Mech.* **213**, 611–639.

Pier, B., Huerre, P., Chomaz, J.-M. & Couairon, A. 1998 Steep nonlinear global modes in spatially developing media. *Phys. Fluids* **10** (10), 2433–2435.

Sevilla, A. 2011 The effect of viscous relaxation on the spatiotemporal stability of capillary jets. *J.Fluid Mech.* **684**, 204–226.

CHAPTER

THREE

Computational Procedure

In order to study the effect of base flow non-parallelism in the stability of low-density jets, we need to compute the evolution of the local absolute growth rate $\omega_{0,i}$ in the streamwise direction for some significant cases.

First, the description of the base flow is obtained by integrating numerically the equations of motion with the boundary-layer and low-Mach number approximations 2.2a–2.2c and appropriate boundary conditions. The axial derivatives of the axial velocity $du/dx(r)$ and the density $d\rho/dx(r)$ need to be obtained then as they are needed for the subsequent stability computations. Once the base flow has been computed, the eigenvalue problem formed by the stability equations after the substitution of the normal modes into the linearized equations of motion (equations 2.8a–2.8d) can be solved for the values of ω and k with a Chebyshev spectral collocation method at each streamwise location and boundary conditions 2.9–2.11. However, we are only interested in the values of ω and k for the wave packet of zero velocity (ω_0,k_0). The condition for the wave packet of zero velocity is that $d\omega/dk(k_0) = 0$, which implies a double root, or a saddle point, in the complex k-plane. An iterative method is implemented numerically to find this saddle point. Furthermore, there are multiple saddle points, but only the one with the highest value of $\omega_{0,i}$ while satisfying the Briggs-Bers criterion (Huerre (2000)) is the one determining the asymptotical behavior of the flow at that location. Once the streamwise distribution of $\omega_{0,i}$ is known, we are able to determine from it the global stability of the flow for a given condition.

The particular numerical methods implemented to solve for the base flow description, the eigenvalue problem and the saddle point determination to obtain (ω_0, k_0) are described in appendices A.1, A.2 and A.3 respectively.

References

Huerre, P. 2000 Open shear flow instabilities. In *Perspectives in fluid dynamics*

(ed. G. Batchelor, K. Moffatt & G. Worster), pp. 159–229. Cambridge.

CHAPTER

FOUR

Results and Discussion

In the present work, some representative cases were analyzed. First, the cases with $S = 0.5$, $D/\theta_0 = 100, 30$ and $Re = 2000, 500, 200$ were studied in order to establish trends in the effect of retaining non-parallel terms of the base flow in the local linear stability analysis. Later, the critical density ratio S_c was computed with and without including the base flow non-parallelism in the computations for the case $D/\theta_0 = 83.5$ and $Re = 2340$. This was done to be able to contrast those results to the experimental evidence of Monkewitz *et al.* (1990).

4.1 Base flow

Figure 4.1 shows the velocity and density profiles obtained for a density ratio $S = 0.5$, $D/\theta_0 = 100$ and $D/\theta_0 = 30$ at different streamwise locations. $D/\theta_0 = 100$ and $D/\theta_0 = 30$ are the representative cases of a flow developing from a velocity profile with a small momentum thickness at the injector exit ($D/\theta_0 = 100$) or a relatively large one ($D/\theta_0 = 30$). In figure 4.1a the axial velocity profiles ($u(r)$) at the injector exit have been represented. For $D/\theta_0 = 100$ the momentum thickness is small, and therefore the axial velocity profile is constant except for a small region near $r = 1$. We can observe that, as expected, the non-constant region for $D/\theta_0 = 30$ is wider than in the previous case as corresponds to a bigger momentum thickness. Past $r = 1$, the axial velocity component is 0 (stagnant ambient) and the density is 2 agreeing with a value of $S = \rho_j/\rho_\infty = 0.5$. Note that the axial velocity component u^*, has been nondimensionalized with $u_j = Q/(\pi a^2)$ so that the axial nondimensional velocity at the center of the jet ($r = 0$) is $u > 1$. We can see for the different values of x in figure 4.1 how the density and axial velocity component profiles get thicker as we advance in the streamwise direction. The axial derivatives of the axial velocity component ($\frac{\mathrm{d}u}{\mathrm{d}x}(r)$) and the density ($\frac{\mathrm{d}\rho}{\mathrm{d}x}$) of the base flow have been computed as well, and are shown in figure 4.2 at different streamwise locations and for the cases $D/\theta_0 = 100, 30$, as they are some of the non-parallel properties of the base flow

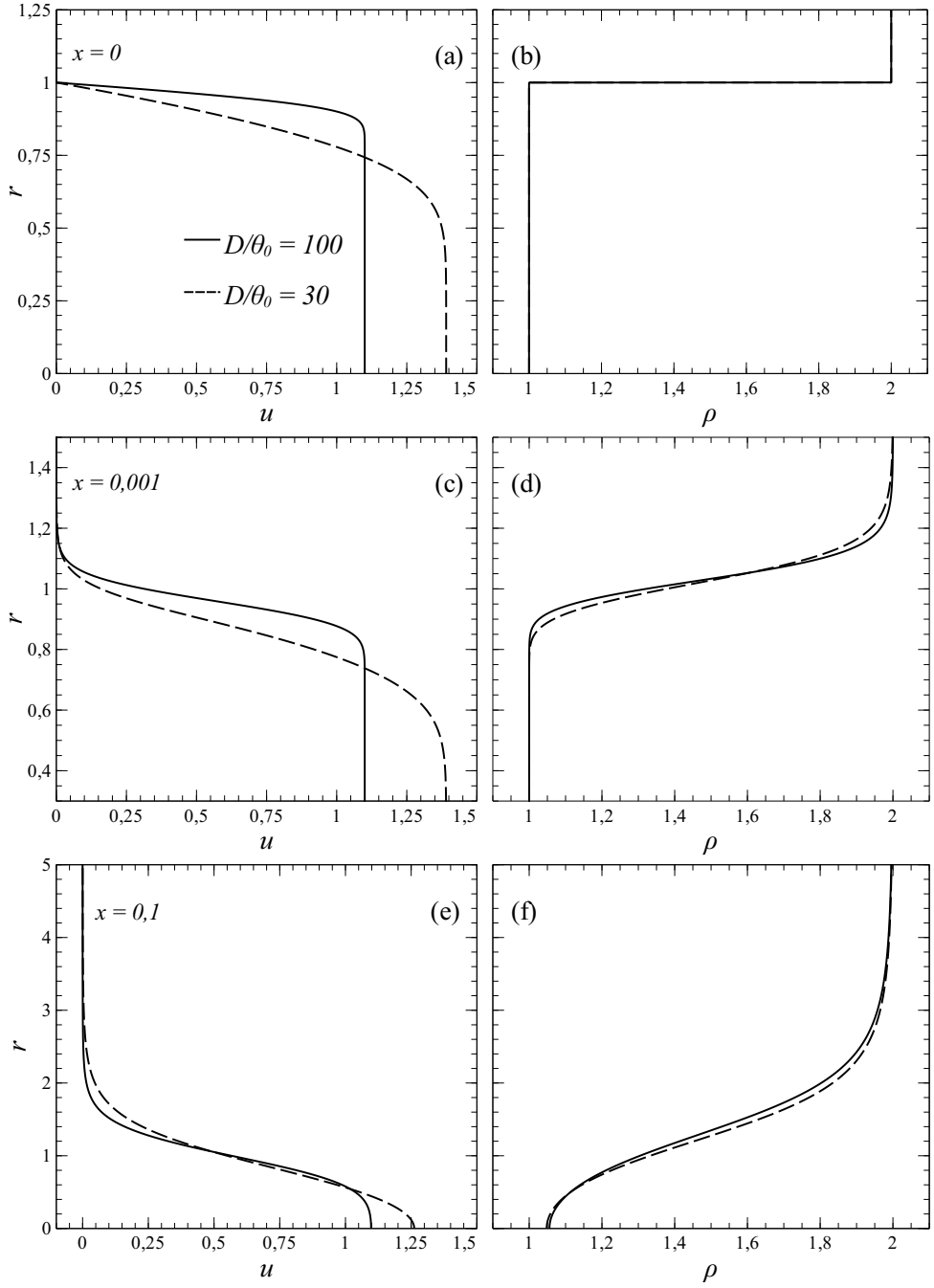

Figure 4.1: Hot jet base flow nondimensional velocity (a),(c),(e) and density (b),(d),(f) profiles at different streamwise locations for a density ratio $S = 0.5$, momentum thickness $D/\theta_0 = 100$(solid lines) and $D/\theta_0 = 30$(dashed lines).

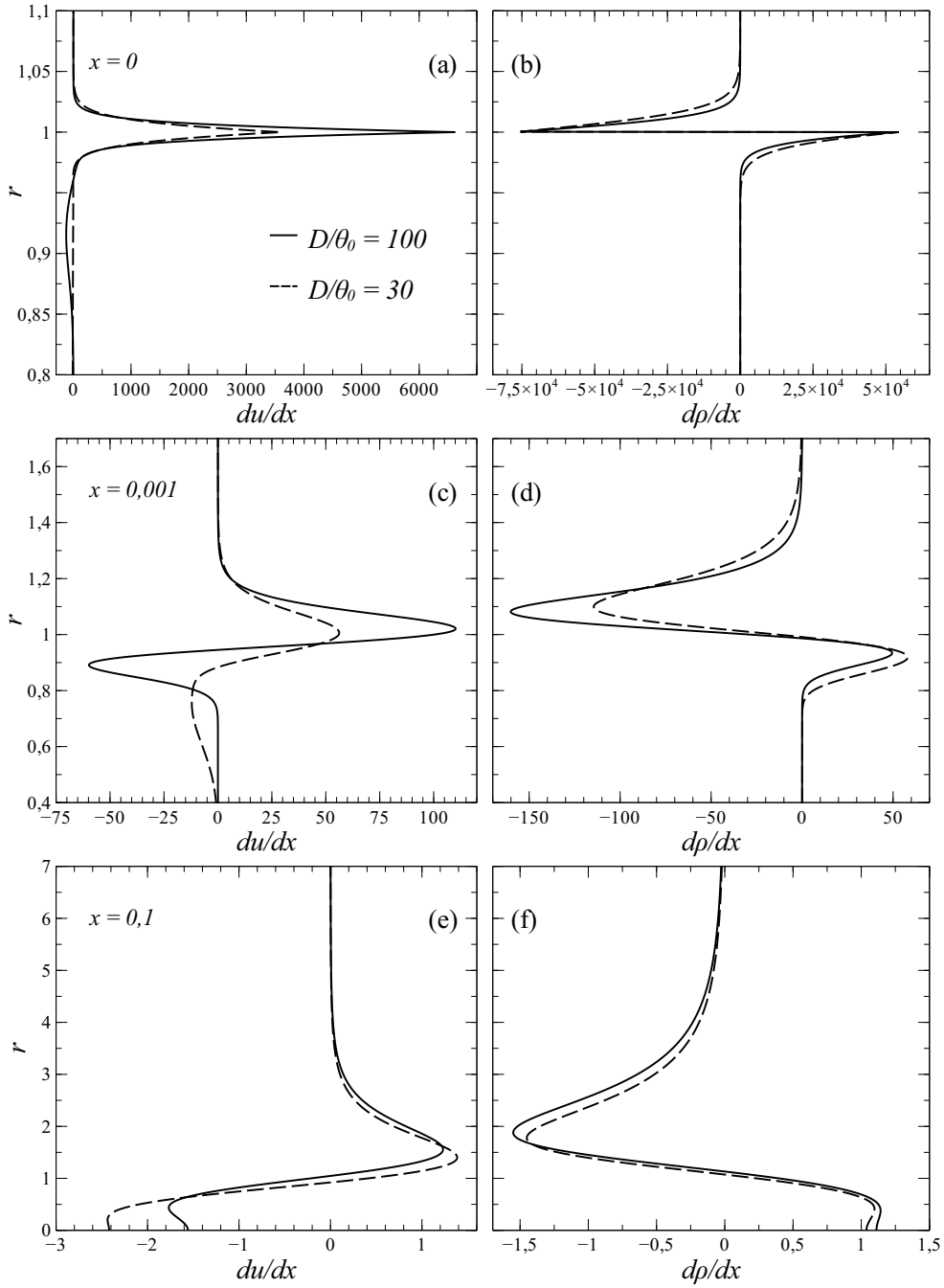

Figure 4.2: Hot jet base flow nondimensional axial velocity derivatives ($du/dx(r)$) (a,c,d) and axial density derivatives($d\rho/dx(r)$) (b,d,f) profiles at different locations of the streamwise coordinate for a density ratio $S = 0.5$, momentum thickness $D/\theta_0 = 100$(solid line) and $D/\theta_0 = 30$(dashed line). Note that the nondimensionalization for the base flow is done with $x \sim Rea$ whereas for the stability analysis $x \sim a$. Therefore, although here the values of du/dx and $d\rho/dx$ may look unreasonably high, those values must be divided by the Reynolds number in order to represent each particular case for different values of Re.

whose effect we want to study including them in the local linear stability analysis of the flow. It is important to note that the seemingly high values for $\frac{du}{dx}$ and $\frac{d\rho}{dx}$ come from the fact that $x^* \sim Re\,a$ in the nondimensionalization of the base flow. Therefore, in order to adjust $\frac{du}{dx}$ and $\frac{d\rho}{dx}$ for each different value of the Reynolds number, we would have to divide the values shown in figure 4.2 by the appropriate Re in each case. The general trend shown by the axial derivatives of the base flow properties ($\frac{du}{dx}$,$\frac{d\rho}{dx}$) is that the closer to the injector exit, the higher their value. Furthermore, the decrease in significance of the axial derivatives from $x = 0$ to $x = 0.001$ is of the same order of magnitude that their decrease from $x = 0.001$ to $x = 0.1$. However, the difference in x is much greater for the later case ($x = 0.001 \rightarrow x = 0.1$). Therefore, the values of the axial derivatives of the base flow as inferred from $\frac{du}{dx}$ and $\frac{d\rho}{dx}$ are higher the closer to the injector exit ($x = 0$), and their decrease along the streamwise coordinate is greater the closer they we get to the injector exit as well.

4.2 Stability

The downstream evolution of the local stability properties for $S = 0.5$ and $D/\theta_0 = 100$ at different Reynolds numbers can be observed in figure 4.3 with and without the effect of base flow non-parallelism. To the right of the figure an overview of the downstream evolution can be seen while a close up view of the evolution near the injector exit is shown to the left. The axial coordinate x divided by the Reynolds is represented in the horizontal axis for both (a) and (b) whereas in the vertical axis the frequency $\omega_{0,r}$ (a) and the absolute growth rate $\omega_{0,i}$ (b) are represented.

It is important to note that the fact that the downstream distributions, past a small region near the injector exit, almost collapse onto a single line when ω is represented versus x/Re validates the previous order of magnitude analysis based on the assumption that characteristic length of the base flow is $Re\,a$.

In general, as it can be observed in the figure, the higher the Reynolds number, the greater the absolute growth rates. Therefore, increasing the Reynolds number has a destabilizing effect on the flow.

The effect of base flow non-parallelism can be seen to have a significant impact in the region closer to the injector exit, up to $x/Re = 0.01$. In this case, independently of the Reynolds number, the effect of the base flow non-parallelism is to stabilize the flow. This means that the local absolute growth rates are reduced, bringing the curves of $\omega_{i,0}$ down from the ones obtained without taking into account base flow non-parallelism. The lower the Reynolds, the greater the

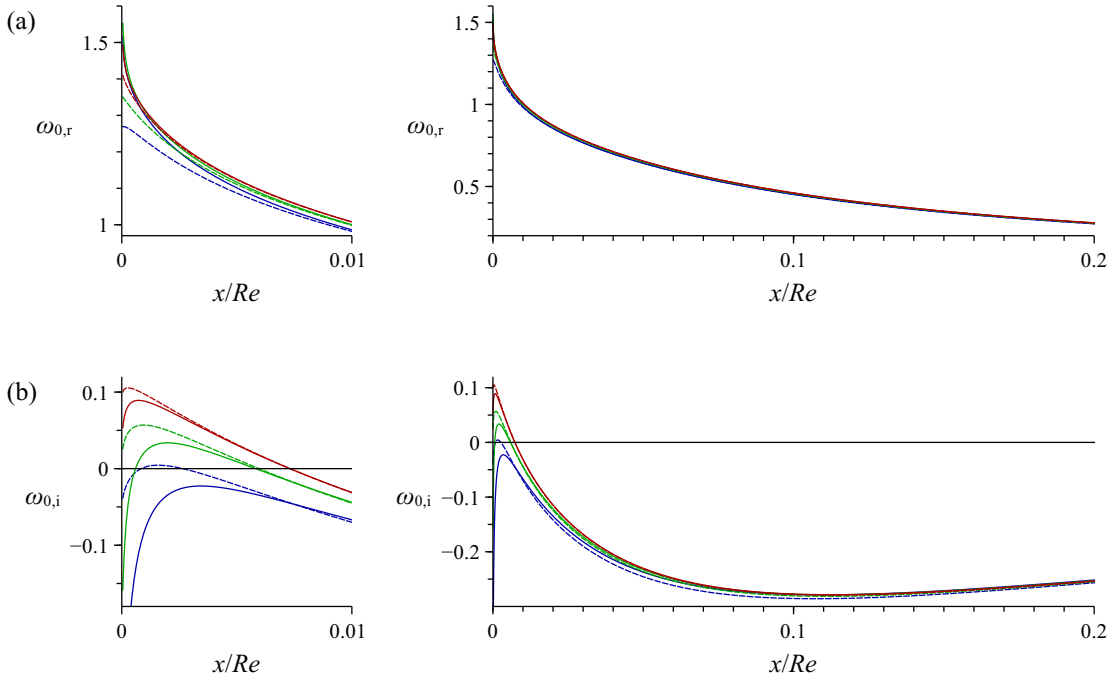

Figure 4.3: Distribution of ω_0 as a function of the streamwise coordinate for $D/\theta_0 = 100$, $S = 0.5$ and Re =2000(red), 500(green), 200(blue). In (a) the frequency $\omega_{0,r}$ is represented whereas in (b) we represent the absolute growth rate $\omega_{0,i}$. On the left column, the region closest to the injector is enlarged from the figure on the right column for a better visualization.

stabilizing effect of including base flow non-parallel terms in the analysis. In fact, for the case in which $Re = 200$, the unstable nature of the flow is changed from globally absolutely unstable to globally convectively unstable by retaining base flow non-parallel terms. Without including the non-parallelism of the base flow, the evolution of $\omega_{0,i}$ for $Re = 200$ presents a pocket of local absolute instability that disappears when taking the base flow non-parallelism into account. Another effect of the addition of base flow non-parallel terms is the downstream delay in the location of the maximum absolute growth rate, as the stabilizing effect of the base flow non-parallelism is greater the closer to the injector exit. This will result in a slower dominant temporal frequency of the flow. The dominant temporal frequency of the flow (ω_r) is the one that can be found at the same location as the maximum value of the growth rate ($\omega_{0,i}$). As the value of ω_r decreases as x increases, if the location of the maximum growth rate is delayed, the dominant temporal frequency will be slower.

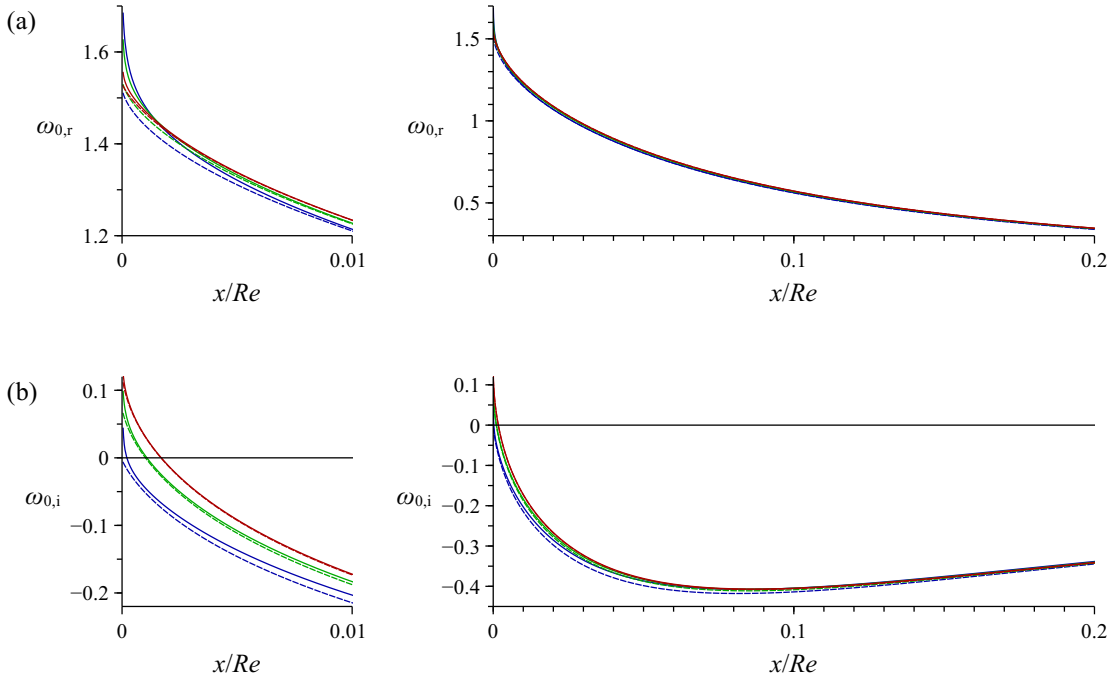

Figure 4.4: Distribution of ω_0 as a function of the streamwise coordinate for $D/\theta_0 = 30$, $S = 0.5$ and $Re = 2000$ (red), 500(greens), 200(blue). In (a) the frequency $\omega_{0,r}$ is represented whereas in (b) we represent the growth rate $\omega_{0,i}$. On the left column, the region closest to the injector is enlarged from the figure on the right column for a better visualization.

The evolution of the local stability properties for the case $D/\theta_0 = 30$ is shown in figure 4.4. For this value of initial momentum thickness (D/θ_0), the effect of retaining the base flow non-parallelism in the analysis is small. However, the trend in the effect of the Reynolds number is the same as for $D/\theta_0 = 100$. This can be observed clearer in the evolution of the frequency (a) than in the evolution of the absolute growth rate (b) as the differences generated by the base flow non-parallelism are greater in the first. The lower the Reynolds number, the bigger the change generated by the retention of base flow non-parallelism. An important difference, influencing the determination of the nature of the global instability between the cases $D/\theta_0 = 30$ and $D/\theta_0 = 100$, is the shape of the evolution of $\omega_{0,i}$. In the case of $D/\theta_0 = 100$ the evolution of $\omega_{0,i}$ is of type II, as described in chapter 2.2.2. Whereas for $D/\theta_0 = 30$ the evolution is of type III. Nevertheless, the main difference is that the effect of retaining base flow non-parallel terms is quite significant for $D/\theta_0 = 100$ while almost negligible

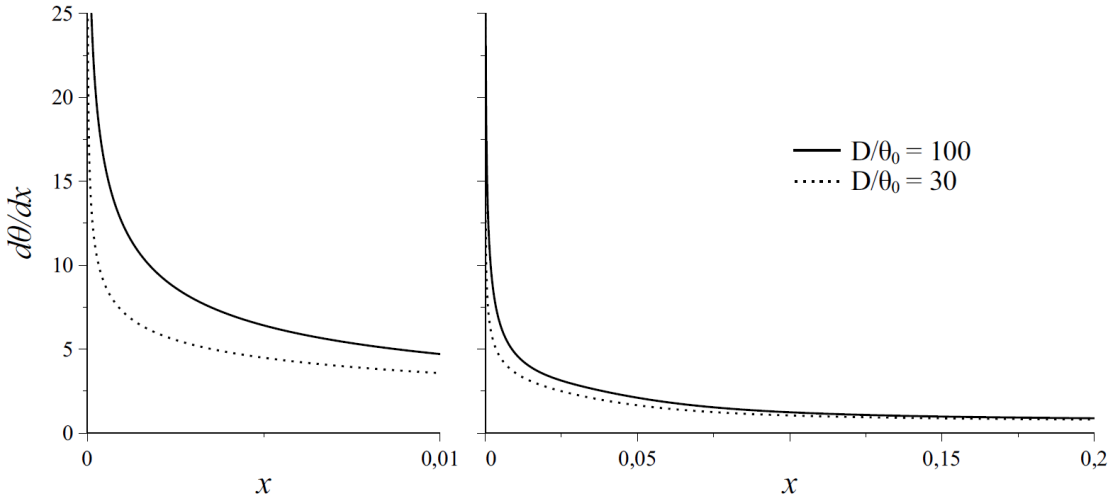

Figure 4.5: Spatial distribution of the axial derivatives of the momentum thickness for the cases $D/theta_0 = 100$ and $D/theta_0 = 30$. On the left column, the region closest to the injector is enlarged from the figure on the right column for a better visualization.

for $D/theta_0 = 30$.

This difference in the relevance of including the non-parallelism of the base flow in the analysis for different initial momentum thicknesses of the base profile, can be explained by the axial variations in momentum thickness near the injector exit. The spatial evolution of the axial derivatives of the momentum thickness (figure 4.5) is a measure of the radial development of the flow. Therefore, the larger the axial derivatives of the momentum thickness near the injector exit, the greater the importance of the base flow non-parallelism in the stability of the flow. In figure 4.5, the spatial distribution of the axial derivatives of the momentum thickness of the base flow is shown for two different values of the ratio D/θ_0, namely $D/\theta_0 = 100$ and $D/\theta_0 = 30$. It can be observed that for the case in which the effect of the non-parallel terms in the stability is greater ($D/\theta_0 = 100$), the axial derivatives of the momentum thickness are greater near the injector exit than those in the case $D/\theta_0 = 30$. It is interesting to realize that, further downstream than $x = 0.01$, the evolution of $\frac{\mathrm{d}\theta}{\mathrm{d}x}$ for both values of D/θ_0 converges. Thus explaining the convergence of the evolution of the local stability properties past $x/Re = 0.01$.

4.2.1 Comparison with experiments

There is not much experimental evidence of self-sustained oscillations in hot round jets. The main experimental work that one can find in the literature on

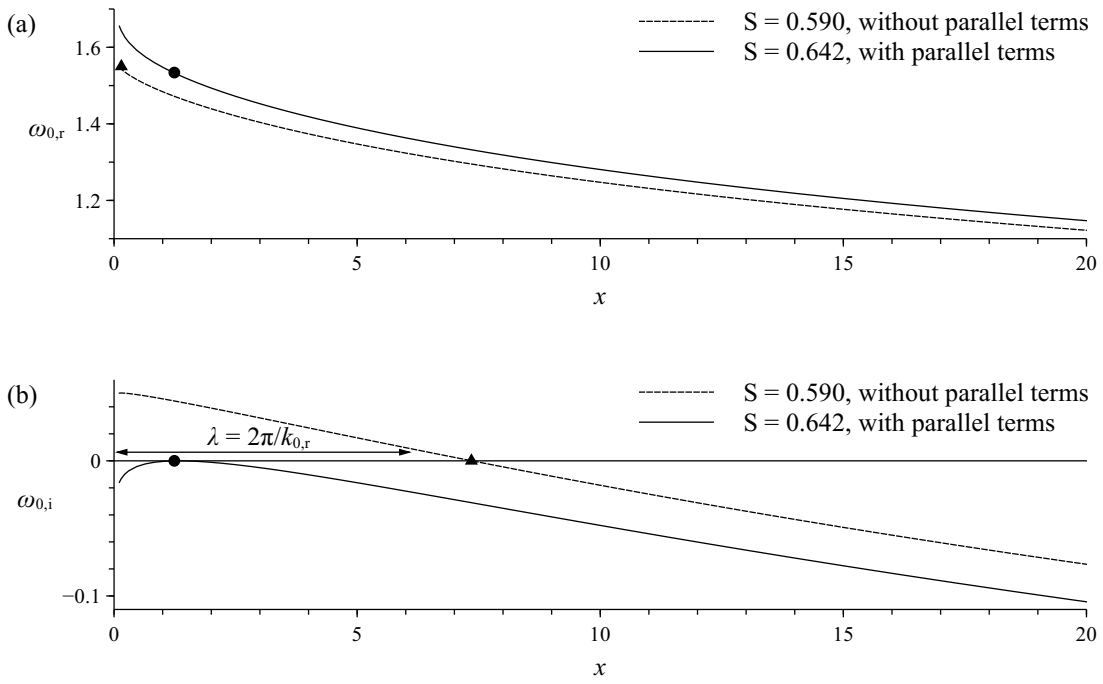

Figure 4.6: ω distribution for $D/\theta_0 = 80$, $Re = 2430$ at the critical values of the density ratio S_c found for the cases with (solid line) and without (dashed lines) non-parallel terms. The filled circle and triangle represent in (b) the points of criticality between absolute and convective instability of the flow for the analysis including(circle) and not(triangle) non-parallel terms. In (a), the filled circle and triangle represent the frequency that will dominate the instability of the flow in each case.

the stability of hot round jets was performed by Monkewitz *et al.* (1990). They studied experimentally the onset of global absolute instability in heated jets. The conditions of their experiment had to be translated to our nondimensionalization, that is different to theirs. Finally, the conditions of their experiment according to our non dimensional variables were found to be $D/\theta_0 = 83.5$ and $Re = 2340$. A detailed account of the transformation process can be found in section 4 of Coenen & Sevilla (2012).

Monkewitz *et al.* (1990) measured the near field pressure spectra of a hot jet, for conditions D/θ_0 and Re mentioned above, and plotted the dominant amplitude for different jet-to-ambient ratios ($S = \rho_j/\rho_\infty$). The squares that can be observed in figure 4.7 represent the nondimensionalized dominant pressure amplitudes recorded during the experiment for what Monkewitz *et al.* (1990) denominated global instability Mode II, which is the one relevant to the present

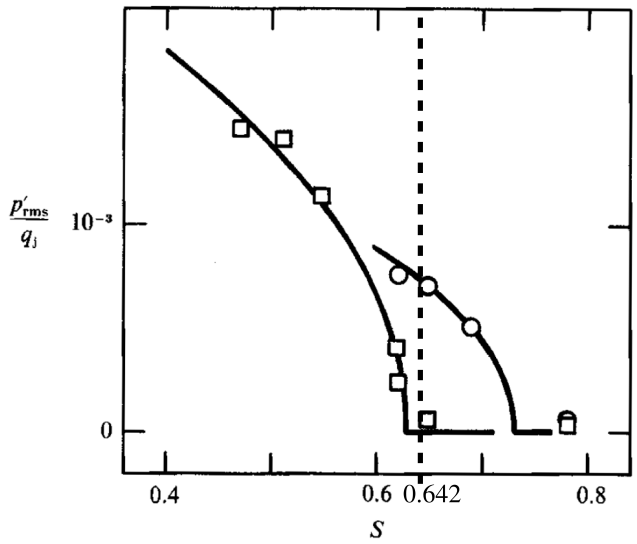

Figure 4.7: Experimental results for the amplitude of oscillations at a fixed $Re = 2340$ compared to the results obtained for a local linear stability analysis that included base flow non-parallellism. The critical density ratio for Mode II in Monkewitz *et al.* (1990) (solid line to the left and squares for scatter data) was found experimentally to be $S_c = 0.63$ whereas when perfoming a local linear stability analysis reatining base flow non-parallelism we found $S_c = 0.642$, which is showed with a vertical dashed line. Original figure taken from Monkewitz *et al.* (1990)

work. A curve, with a profile coming from a Landau equation (see Monkewitz *et al.* (1990) and referenced therein), was fitted to those data points yielding a critical density ratio $S_c = 0.63$ below which the flow presented Mode II self-sustained oscillations.

A local linear stability analysis was performed in order to compare the resulting critical density ratio to the one found experimentally, and to determine whether retaining base flow non-parallelism increased the accuracy of the result. Figure 4.6 shows the downstream evolution of the local stability properties for the limiting cases of critical density ratio, S_c, found in our computations. The solid lines represent the analysis retaining base flow non-parallelism while the dashed lines represent the analysis without taking those terms into account. The filled circle and triangle represent the points of criticality for the criteria to go from convective to absolute instability in figure 4.6b and the frequency that will dominate the flow in figure 4.6a. It is important to note that the evolution of the absolute growth rate, $\omega_{0,i}$ (Figure 4.6b), is found to be of a different type, as explained in chapter 2.2.2, for the case computed including base flow non-parallelism (type II) than for the case in which the non-parallelism of the base

flow was not taken into account (type III). This difference in the type of evolution of $\omega_{0,i}$ affects the criteria to determine when global absolute instability is triggered. For an evolution of the absolute growth rate of type II, the onset of global absolute instability occurs when the maximum value of $\omega_{0,i}$ reaches 0. However, in evolutions of the absolute growth rate of type III, the pocket of local absolute instability must reach a certain length in order for the flow to become globally absolutely unstable. In this work the criteria used to determine that critical length was for it to be equal to the wave length of the frequency at the injector exit. This is why the filled triangle in figure 4.6b is located at $x = 7.5$.

The critical density ratios, S_c, found using the criteria described before, were $S_c = 0.590$ for the case in which non-parallel terms of the base flow where not included in the analysis and $S_c = 0.642$ for the case in which non-parallel terms of the base flow were included. As can be inferred from comparing those values with the experimental one $S_c = 0.63$, the retention of base flow non-parallelism in the stability analysis increased its accuracy. In figure 4.7 it can be observed graphically how close the resulting critical value obtained retaining base flow non-parallelism is to the experimental one. A vertical dashed line indicates where our result falls compared to the experimental one.

References

Coenen, Wilfried & Sevilla, A. 2012 The structure of the absolutely unstable regions in the near field of low-density jets. *J. Fluid Mech.* **713**, 123–149.

Monkewitz, P. A., Bechert, D. W., Barsikow, B. & Lehmann, B. 1990 Self-excited oscillations and mixing in a heated round jet. *J. Fluid Mech.* **213**, 611–639.

CHAPTER

FIVE

Conclusions

When performing a local linear spatiotemporal stability analysis of hot round jets at moderate Reynolds numbers, non-parallelism of the base flow is typically neglected. In the present work non-parallelism was found to be present in certain terms that are of an order of magnitude significant enough to be taken into account for the stability analysis. Therefore, local linear spatiotemporal stability analysis has been performed with and without taking those non-parallel terms into account. This way the influence that those non-parallel terms have into the local and, eventually, global stability of the flow can be studied.

The evolution of the local absolute growth rate for the wave packet of zero velocity $\omega_{0,i}(x)$, was obtained for the cases of a density ratio $S = 0.5$, different values of the momentum thickness of the velocity profile at the injector outlet $D/\theta_0 = 100$ and 30, and considering the range of Reynolds numbers $Re = 2000, 500, 200$. Furthermore, the critical density ratio Sc was computed for $D/\theta_0 = 83.5$ and $Re = 2340$ in order to contrast the results with the experimental ones of Monkewitz *et al.* (1990).

It has been found that non-parallel terms play a significant role in the stability of the near field of hot round jets and they should not be neglected without a loss of accuracy. In some occasions, as can be seen in figure 4.3, the introduction of those non-parallel terms is crucial as it changes completely the nature of the global stability of the flow, from globally absolutely unstable to globally convectively unstable. Furthermore, from the results obtained, one can conclude that the effect of non-parallel terms in the stability of hot jets is greater the higher the value of D/θ_0. Additionally, it has been observed that as the Reynolds number increases, the effect of non-parallelism is reduced.

The main conclusion of the present work comes from the comparison of the local linear spatiotemporal stability analysis performed with the experimental results of Monkewitz *et al.* (1990). The insertion of the base flow non-parallel terms allows to improve the accuracy of the stability analysis from a critical densitity ratio of 0.590 to that of 0.642 when the experimental value found was 0.630. Most importantly, the inclusion of base flow non-parallelism into

the analysis not only allows for an increased accuracy, but it changes in this case the shape of the spatial evolution of the absolute growth rate ($\omega_{0,i}$) from type III to type II (see chapter 2.2.2 for the different types of spatial evolution for the absolute growth rate), as can be seen in figure 4.6. This change in the spatial evolution of the absolute growth rate has important repercussions in the determination of global instability. In the cases in which the addition of base flow non-parallelism results in a change of the spatial evolution of the absolute growth rate from type III, in figure 2.3, to type II, the determination of global instability can be done making use of the criteria associated to type II absolute growth rate evolutions which is theoretically more sound than the ones associated to type III evolutions. This would greatly improve the determination of the global stability properties of flows that now present local absolute growth rate evolutions of type III.

Future prospects

In the present work, the effect of base flow non-parallelism in the linear local spatiotemporal stability analysis of hot jets has been studied. The results obtained present a good correlation with the experiment by Monkewitz *et al.* (1990). This results seem promising, however the lack of experimental data for hot jets does not allow for a thorough validation of the methodology. Nevertheless, here only hot jets have been analyzed. There is much more experimental evidence of self-excited oscillatory behavior in light jets. As both hot and light jets are low-density jets and present analogous flow structures, though not equal, we expect the trends in the effect of base flow non-parallelism on local stability properties to be similar in both cases. Therefore, the aim is to implement a local linear spatiotemporal stability analysis for light jets retaining the effect of base flow non-parallelism, employing the same methodology as the one used in the present work, in order to be able to contrast the results with the wider range of existing light jet experiments.

References

Monkewitz, P. A., Bechert, D. W., Barsikow, B. & Lehmann, B. 1990 Self-excited oscillations and mixing in a heated round jet. *J. Fluid Mech.* **213**, 611–639.

APPENDIX

A

Numerical methods

The codes containing the numerical methods implemented for the obtention of solutions to the base flow and to the stability problem were not developed by the author of the present work. The author simply adapted the codes used by Coenen (2010) to the specific needs that motivated the present work. Namely, additions were done to the computation of the base flow in order to record the axial derivatives of base flow properties as they were needed for the later stability analysis. The code that solves the stability equations was modified as well in order to take into account base flow non-parallelism. Section A.4 contains extracts of the code where the main modifications were done with respect to the original. The other sections of the appendix, which describe the numerical methods implemented in the codes used, have been taken from Coenen (2010), with permission from its author, and modified accordingly to fit the needs of the present work.

A.1 Numerical integration of the jet flow

To find a numerical solution of the parabolic boundary-layer equations (2.2a)–(2.2c), that describe the jet flow field, we have used a fully implicit marching procedure in the streamwise x-direction, applying second-order accurate finite difference schemes. The equations are discretized on the points of a non-uniform grid, carefully designed to cluster grid point axially near the entrance of the jet at $x = 0$ and radially around the jet shear layer at $r = 1$. For this purpose, we use grid transformations proposed by Roberts (1971) that map the uniformly distributed computational domains $\xi \in [0,1]$, $\eta \in [0,1]$ on the non-uniform physical domains $x \in [0, x_{\max}]$, $r \in [0, r_{\max}]$:

$$\begin{cases} x = 1 + (x_{\max} - 1)\dfrac{(\tau_x+1)-(\tau_x-1)\frac{\tau_x+1}{\tau_x-1}^{1-\eta}}{1+\frac{\tau+1}{\tau-1}^{1-\eta}}, \\ \xi = 1 - \dfrac{\ln \frac{\tau_x+1-x/x_{\max}}{\tau_x-1+x/x_{\max}}}{\ln \frac{\tau_x+1}{\tau_x-1}}, \end{cases} \tag{A.1a}$$

and

$$\begin{cases} r = \dfrac{(\beta+2\alpha)\left(\frac{\beta+1}{\beta-1}\right)^{\frac{r_{\max}\eta/Q-\alpha}{1-\alpha}} - \beta + 2\alpha}{(2\alpha+1)\left[1+\left(\frac{\beta+1}{\beta-1}\right)^{\frac{r_{\max}\eta/Q-\alpha}{1-\alpha}}\right]} \\ \eta = \dfrac{Q}{r_{\max}}\left[\alpha + (1+\alpha)\dfrac{\ln\frac{\beta+r(2\alpha+1)-2\alpha}{\beta-r(2\alpha+1)+2\alpha}}{\ln\frac{\beta+1}{\beta-1}}\right] \end{cases} \quad \left(0 \le \eta \le \frac{Q}{r_{\max}},\ 0 \le r \le 1\right), \tag{A.1b}$$

$$\begin{cases} r = 1 + (r_{\max}-1)\dfrac{(\tau+1)-(\tau-1)\left(\frac{\tau+1}{\tau-1}\right)^{1-\frac{\eta-Q/r_{\max}}{1-Q/r_{\max}}}}{1+\left(\frac{\tau+1}{\tau-1}\right)^{1-\frac{\eta-Q/r_{\max}}{1-Q/r_{\max}}}} \\ \eta = \dfrac{Q}{r_{\max}} + \left(1+\dfrac{Q}{r_{\max}}\right)\left[1 - \dfrac{\ln\frac{\tau+1-(r-1)/(r_{\max}-1)}{\tau-1+(r-1)/(r_{\max}-1)}}{\ln\frac{\tau+1}{\tau-1}}\right] \end{cases} \quad \left(\frac{Q}{r_{\max}} \le \eta \le 1,\ 1 \le r \le r_{\max}\right). \tag{A.1c}$$

In the calculations we have used $N_x = 1000$ grid points in the axial direction, with $x_{\max} = 0.0025$ and $\tau_x - 1 = 0.02$, and $N_r = 5000$ grid points in the radial direction, with $r_{\max} = 1000$, $Q = 100$, $\tau - 1 = 5.32 \times 10^{-6}$ and $\beta - 1 = 0.001$.

In the computational domain, we apply a second-order accurate backward finite-difference formula

$$\left.\frac{\partial\phi}{\partial\xi}\right|_j^{i+1} \simeq \frac{3\phi_j^{i+1} - 4\phi_j^i + \phi_j^{i-1}}{2\Delta\xi} \tag{A.2}$$

in the axial ξ-direction and second-order accurate central-difference schemes

$$\left.\frac{\partial\phi}{\partial\eta}\right|_j^{i+1} \simeq \frac{\phi_{j+1}^{i+1} - \phi_{j-1}^{i+1}}{2\Delta\eta} \quad \text{and} \quad \left.\frac{\partial\phi}{\partial\eta}\right|_j^{i+1} \simeq \frac{\phi_{j+1}^{i+1} + 2\phi_j^{i+1} - \phi_{j-1}^{i+1}}{(\Delta\eta)^2} \tag{A.3}$$

in the radial η direction.

At each step in the marching procedure, an iterative process is carried out, in which we subsequently solve a linearized form of the momentum and energy equations for u and T, followed by the solution of the continuity equation to obtain v, using the newly calculated values of u and T. At each iteration step, the flow variables that are used in the linearization are updated with the solution that was found in the last completed step. This process is continued until convergence is achieved, here defined to be when $\{\sum_{j=1}^{N_r}(\phi - \tilde{\phi})_{i,j}^2 / \sum_{j=1}^{N_r}\tilde{\phi}_{i,j}^2\}^{1/2}$ falls below a prescribed tolerance of 10^{-6} for all flow variables ϕ.

A.2 Chebyshev spectral collocation method

The generalized eigenvalue problem set up by the system of ordinary differential equations (2.8a)–(2.8d) with boundary conditions (2.9)–(2.11) can be solved with a Chebyshev spectral collocation method.

When a complex frequency ω needs to be computed for a given complex wavenumber k, the eigenvalue problem is written as

$$\mathbf{A}\boldsymbol{x} = \omega\mathbf{B}\boldsymbol{x}\,, \tag{A.4}$$

where $\boldsymbol{x} = (\hat{\rho}, \hat{u}, \hat{v}, \hat{w}, \hat{p})$, and $\mathbf{A}$ and $\mathbf{B}$ are two linear operators.

Following Khorrami *et al.* (1989), the eigenfunctions $(\hat{\rho}, \hat{u}, \hat{v}, \hat{w}, \hat{p})$ are mapped from the physical domain $0 \le r \le r_{\max}$ onto the Chebyshev interval $-1 \le \xi \le 1$, where they are discretized in N collocation points,

$$\xi_j = \cos\left(\frac{j\pi}{N-1}\right), \quad j = 0, \ldots, N-1\,. \tag{A.5}$$

For this purpose, we use the transformation proposed by Lesshafft & Huerre (2007)

$$\xi(r) = \frac{r_c}{2r} - \left(1 + \frac{r_c^2}{4r^2} + \frac{2r_c}{r_{\max}} - \frac{r_c}{r}\right)^{1/2}, \tag{A.6a}$$

$$r(\xi) = r_c \frac{1-\xi}{1-\xi^2 + 2r_c/r_{\max}}\,. \tag{A.6b}$$

In this way, approximately half of the points $r_j = r(\xi_j)$ are placed in the interval $0 \le r \le r_c$, concentrated around $r = r_c/2$. For the jet profiles considered in this dissertation, values $r_c = 2$ and $r_{\max} = 1000$ were found satisfying. A minimum number of $N = 128$ collocation points was used, increasing this number for profiles with thin shear layers so that a minimum of 10 collocation points are placed within the high-gradient regions of the velocity and density profiles.

The linear operators $\mathbf{A}$ and $\mathbf{B}$ of the eigenvalue problem (A.4) are $5N \times 5N$-matrices containing $5(N-1)$ lines with the five stability equations discretized in the $N-1$ interior nodes, and $10N$ lines representing the boundary conditions at the extremes of the Chebyshev domain. To compute ω in the generalized eigenvalue problem (A.4), we use the ZGGEV routine from the LAPACK linear algebra library.

If a complex wavenumber k needs to be computed for a given complex frequency ω, we can write the eigenvalue problem as

$$[\mathbf{A} - k\mathbf{B_1} - k^2\mathbf{B_2}]\boldsymbol{x} = 0\,, \tag{A.7}$$

which can be converted into the linear eigenvalue problem

$$\mathbf{M_A} z = k \mathbf{M_B} z, \tag{A.8}$$

where $z = (\boldsymbol{x}, k\boldsymbol{x}) = (\hat{\rho}, \hat{u}, \hat{v}, \hat{w}, \hat{p}, k\hat{\rho}, k\hat{u}, k\hat{v}, k\hat{w}, k\hat{p})$,

$$\mathbf{M_A} = \begin{bmatrix} \mathbf{0} & \mathbf{I} \\ \mathbf{A} & -\mathbf{B_1} \end{bmatrix} \quad \text{and} \quad \mathbf{M_B} = \begin{bmatrix} \mathbf{I} & \mathbf{0} \\ \mathbf{0} & \mathbf{B_2} \end{bmatrix}. \tag{A.9}$$

This system can be solved as described above. Note that now the matrices $\mathbf{M_A}$ and $\mathbf{M_B}$ are significantly larger, counting $10N \times 10N$ elements, and consequently the computational cost significantly higher.

A.3 Saddle point determination

In the surroundings of the saddle point (ω_0, k_0), the frequency $\omega(k)$ as a function of the wavenumber k admits a quadratic Taylor expansion around k_0,

$$\omega(k) = \omega_0 + l(k - k_0)^2. \tag{A.10}$$

This can be exploited in an iterative procedure to find the location of (ω_0, k_0) as follows. We choose three wavenumbers k_1, k_2, k_3 around an initial guess k_0^* with

$$k_n = k_0^*(1 + \varepsilon\, \mathrm{e}^{\mathrm{i}2\pi(n-1)/3}) \qquad (n = 1, 2, 3), \tag{A.11}$$

where ε is a distance small enough for k_n to fall in the region where the quadratic approximation of $\omega(k)$ is valid. We then solve the eigenvalue problem for each of the k_n using the spectral collocation method described in the previous section, yielding three frequencies ω_1, ω_2 and ω_3. Now the three pairs (ω_n, k_n) can be used in a Newton-Raphson method to find (ω_0, k_0) and l that make the quadratic approximation (A.10) fit or, in other words, to find the saddle point. That is, we search the zero $\boldsymbol{x} = [\omega_0, k_0, l]$ of the function

$$\boldsymbol{F}(\boldsymbol{x}) = \begin{bmatrix} \omega_1 - \omega_0 - l(k_1 - k_0)^2 \\ \omega_2 - \omega_0 - l(k_2 - k_0)^2 \\ \omega_3 - \omega_0 - l(k_3 - k_0)^2 \end{bmatrix}. \tag{A.12}$$

With the newly obtained value of k_0, three new values of k_1, k_2 and k_3 are calculated using (A.11), and the quadratic fitting is repeated. This iterative procedure is repeated until relative differences in (ω_0, k_0) between subsequent iteration steps fall below 10^{-5}. At each step ε is slightly decreased to enhance the accuracy of the procedure.

Note that this method takes advantage of the linearity of the eigenvalue problem in ω. A similar method was formulated by Monkewitz & Sohn (1988), but they proposed an expansion of $k(\omega)$, in this way necessitating the solution of the quadratic eigenvalue problem in k. In the previous section we saw that this implies a higher computational cost.

A.4 Main modifications to original code

There are two main modifications to the original codes as mentioned above. One is the computation of $\frac{\mathrm{d}u}{\mathrm{d}x}$ and $\frac{\mathrm{d}\rho}{\mathrm{d}x}$ for the base flow and the other is the introduction of the non-parallel terms in the matrices **A** and **B** that define the eigenvalue problem.

Computation of axial derivatives of the base flow

The computation of $\frac{\mathrm{d}u}{\mathrm{d}x}$ and $\frac{\mathrm{d}\rho}{\mathrm{d}x}$ for the base flow was not implemented in the original code as non-parallelism of the base flow was not retained into the stability analysis. Therefore, two subroutines needed to be introduced in order to compute $\frac{\mathrm{d}u}{\mathrm{d}x}$ and $\frac{\mathrm{d}\rho}{\mathrm{d}x}$. This was achieved by means of a first-order backward-difference method as can be seen in listing A.1 at the end of this section.

Modification of the code which solves the eigenvalue problem

The code that solves the eigenvalue problem needed to be modified to take into account the base flow non-parallel terms. The author of the present work had to input those terms into the stability matrices **A** and **B** from the eigenvalue problem ($\boldsymbol{A}\,\boldsymbol{x} = \omega \boldsymbol{B}\,\boldsymbol{x}$), where $\boldsymbol{x} = [\hat{\rho}\,\hat{u}\,\hat{v}\,\hat{p}]'$, formed by equations 2.8a–2.8d. It is important to note that this problem is not the one the code solves, as the code solves for the general eigenvalue problem where azimuthal perturbations $\hat{w}$ are considered, $\boldsymbol{x} = [\hat{\rho}\,\hat{u}\,\hat{v}\,\hat{w}\,\hat{p}]'$. However, as we are not considering azimuthal perturbations in our analysis, the value of m in the following code will be zero.

A piece of the updated code is shown in listing A.2 (at the end of this section), where the non-parallel terms can be seen already in the stability matrices multiplied by the variable CNP. CNP a flag variable, with values 0 or 1. When $CNP = 0$, only base flow strictly parallel terms are used in the computation of the local stability properties. However, when $CNP = 1$ base flow non-parallel terms take part in the computation of the stability properties. Thus allowing for a simple way to change between both types of analysis.

The boundary conditions at the center of the jet had to be modified as well in order to account for base flow non-parallelism. Equation 2.11 was implemented in the code as can be seen in listing A.3.

Listing A.1: Code extract showing how $\frac{\mathrm{d}u}{\mathrm{d}x}$ and $\frac{\mathrm{d}\rho}{\mathrm{d}x}$ are computed

```
subroutine sub_solve_dudx(i)
use mod_var_sol
use mod_var_grid
implicit none
integer :: i
if ( i == 2 ) then
          dudx_i= (u_i-u_i1)/(x(i))
     else
          dudx_i= (3*u_i-4*u_i1+u_i2)/(x(i)-x(i-2))
end if
end subroutine sub_solve_dudx

subroutine sub_solve_drhodx(i)
use mod_var_sol
use mod_var_grid
implicit none
integer :: i
if ( i == 2 ) then
          drhodx_i= (rho_i-rho_i1)/(x(i))
     else
          drhodx_i= (3*rho_i-4*rho_i1+rho_i2)/(x(i)-x(i-2))
end if
end subroutine sub_solve_drhodx
```

Listing A.2: Code extract showing the updated $\boldsymbol{A}$ and $\boldsymbol{B}$ matrices

```
CASE (1)                              ! AXISYMMETRIC:

! Blocks of matrix A:
!
!      [A11,A12,...,A15]
!      [A21,A22,...,A25]
! A =  [A31,A32,...,A35]
!      [A41,A42,...,A45]
!      [A51,A52,...,A55]
```

```
A11= k*U_d*r_d + CNP*(-zi*(V_d + Vp_d*r_d + dUdx_d*r_d    &
     +matmul(V_d*r_d,SD1)))
A12= k*rhob_d*r_d                                          &
     +CNP*( -zi*( drhodx_d*r_d ) )
A13= matmul(rhob_d*r_d,SD1) + rhob_d+rhobp_d*r_d
A14= m*rhob_d
A15= OO

A21= -1.0_wp/Re*(matmul(Up_d*r_d**2,f1)                    &
     +matmul(Upp_d*r_d**2+ Up_d*r_d,f0))                   &
     +CNP*( U_d*dUdx_d*r_d**2 + V_d*Up_d*r_d**2 )
A22= -1.0_wp/Re*(matmul(mub_d*r_d**2,SD2)                  &
     +matmul(mubp_d*r_d**2+mub_d*r_d,SD1) - m**2*mub_d ) &
     +k*zi*rhob_d*U_d*r_d**2 +                             &
     1.0_wp/Re*k**2*4.0_wp/3.0_wp*mub_d*r_d**2             &
     +CNP*( rhob_d*dUdx_d*r_d**2                           &
     +matmul(rhob_d*V_d*r_d**2,SD1) )
A23= zi*rhob_d*Up_d*r_d**2                                 &
     +1.0_wp/Re*(matmul(1.0_wp/3.0_wp*k*mub_d*r_d**2,SD1)&
     +k*mubp_d*r_d**2+1.0_wp/3.0_wp*k*mub_d*r_d )
A24= 1.0_wp/Re*1.0_wp/3.0_wp*k*m*mub_d*r_d
A25= k*zi*r_d**2

A31= -1.0_wp/Re*matmul(k*Up_d*r_d**2,f0)
A32= -1.0_wp/Re*(matmul(1.0_wp/3.0_wp*k*mub_d*r_d**2,SD1)&
     -2.0_wp/3.0_wp*k*mubp_d*r_d**2 )
A33= -1.0_wp/Re*( matmul(4.0_wp/3.0_wp*mub_d*r_d**2,SD2) &
     +matmul(4.0_wp/3.0_wp*(mubp_d*r_d**2+mub_d*r_d),SD1)&
     -(2.0_wp/3.0_wp*mubp_d*r_d                            &
     +4.0_wp/3.0_wp*mub_d+(m**2*mub_d)) )                  &
     +zi*k*rhob_d*U_d*r_d**2+1.0_wp/Re*k**2*mub_d*r_d**2 &
     +CNP*( rhob_d*Vp_d*r_d**2                             &
     +matmul(rhob_d*V_d*r_d**2,SD1) )
A34= (-1.0_wp/Re*( matmul(1.0_wp/3.0_wp*m*mub_d*r_d,SD1) &
     -(2.0_wp/3.0_wp*m*mubp_d*r_d+7.0_wp/3.0_wp*m*mub_d)))
A35= -matmul(zi*r_d**2,SD1)

A41= OO
A42= (1.0_wp/Re*(1.0_wp/3.0_wp*k*m*mub_d*r_d))
A43= (1.0_wp/Re*( matmul(1.0_wp/3.0_wp*m*mub_d*r_d,SD1)  &
```

```
      + (m*mubp_d*r_d + 7.0_wp/3.0_wp*m*mub_d) ))
A44= (1.0_wp/Re*( -matmul(mub_d*r_d**2,SD2)                    &
      -matmul(mubp_d*r_d**2+mub_d*r_d,SD1)                     &
      +mubp_d*r_d+4.0_wp/3.0_wp*m**2*mub_d+mub_d)              &
      +zi*k*rhob_d*U_d*r_d**2                                  &
      +1.0_wp/Re*k**2*mub_d*r_d**2)
A45= (zi*m*r_d)

A51= 1.0_wp/(Re*Pr)*( matmul(Tbp_d*r_d**2,f1)                  &
      +matmul(Tbpp_d*r_d**2+Tbp_d*r_d,f0) )                    &
      +1.0_wp/(Re*Pr)*( matmul(mub_d*r_d**2,g2)                &
      +matmul(mubp_d*r_d**2+mub_d*r_d,g1)                      &
      -matmul(m**2*mub_d,g0) )                                 &
      -matmul(zi*k*rhob_d*U_d*r_d**2                           &
      +1.0_wp/(Re*Pr)*k**2*mub_d*r_d**2,g0)                    &
      +CNP*( -U_d*dTdx_d*r_d**2-V_d*Tbp_d*r_d**2               &
      -matmul(rhob_d*V_d*r_d**2,g1) )
A52= CNP*( -rhob_d*dTdx_d*r_d**2 )
A53= -zi*rhob_d*Tbp_d*r_d**2
A54= OO
A55= OO


! Blocks of matrix B:
!
!      [B11,B12,...,B15]
!      [B21,B22,...,B25]
! B =  [B31,B32,...,B35]
!      [B41,B42,...,B45]
!      [B51,B52,...,B55]

B11= r_d
B12= OO
B13= OO
B14= OO
B15= OO

B21= OO
B22= zi*rhob_d*r_d**2
B23= OO
```

```
B24= OO
B25= OO

B31= OO
B32= OO
B33= zi*rhob_d*r_d**2
B34= OO
B35= OO

B41= OO
B42= OO
B43= OO
B44= zi*rhob_d*r_d**2
B45= OO

B51= - matmul(zi*rhob_d*r_d**2,g0)
B52= OO
B53= OO
B54= OO
B55= OO
```

Listing A.3: Code extract showing the updated boundary conditions for the eigenvalue problem

```
! Boundary conditions at the jet centerline r = 0:
CASE (1)                          ! AXISYMMETRIC:

IF (m == 0) THEN                  ! for m = 0:

  ! mub*T'(0) + Tb'mu(0) = 0:

  Ftmp      = matmul(mub_d,g1) + matmul(Tbp_d,f0)
  F11(1:N)  = Ftmp(1,1:N)
  F12       = OO_v
  F13       = OO_v
  F14       = OO_v
  F15       = OO_v

  ! mub*u'(0) + U'*mu(0) = 0:

  Ftmp      = matmul(Up_d,f0)
```

```
F21(1:N) = Ftmp(1,1:N)
Ftmp     = matmul(mub_d,SD1)
F22(1:N) = Ftmp(1,1:N)
F23      = OO_v
F24      = OO_v
F25      = OO_v

! v(0) = 0:

F31      = OO_v
F32      = OO_v
F33      = IO_v
F34      = OO_v
F35      = OO_v

! w(0) = 0:

F41      = OO_v
F42      = OO_v
F43      = OO_v
F44      = IO_v
F45      = OO_v

! Re*i*p'(0)+2*mub*v''(0)+(2/3*mub'-Re*rhob*V)*v'(0)
!    -2*k/3*(mub*u'(0)+mub'*u(0)) = 0:

F51      = OO_v
Ftmp     = - 2.0_wp/3.0_wp*k*(matmul(mub_d,SD1)+mubp_d)
F52(1:N) = Ftmp(1,1:N)
Ftmp     = 2.0_wp*matmul(mub_d,SD2)   &
+2.0_wp/3.0_wp*matmul(mubp_d,SD1) &
+ CNP*( matmul(-Re*rhob_d*V_d,SD1) )
F53(1:N) = Ftmp(1,1:N)
F54      = OO_v
Ftmp     = Re*zi*SD1
F55(1:N) = Ftmp(1,1:N)
```

References

Coenen, W. 2010 Absolute instability in the near field of low-density jets. PhD thesis, Universidad Carlos III de Madrid.

Khorrami, M. R., Malik, M. R. & Ash, R. L. 1989 Applications of spectral collocation techniques to the stability of swirling flows. *J. Comput. Phys.* **81**, 206.

Lesshafft, L. & Huerre, P. 2007 Linear impulse response in hot round jets. *Phys. Fluids* **19** (2), 024102.

Monkewitz, P. A. & Sohn, K. D. 1988 Absolute instability in hot jets. *AIAA J.* **28**, 911–916.

Roberts, G. O. 1971 Computational meshes for boundary layer problems. In *Lecture Notes in Physics 8*, , vol. 61, pp. 171–177. Proc. Second Int. Conf. Num. Methods Fluid Dyn., Springer, Berlin.

Alphabetical list of references

Batchelor, G. K. & Gill, A. E. 1962 Analysis of the stability of axisymmetric jets. *J. Fluid Mech.* **14**, 529–551.

Briggs, R. J. 1964 *Electron-stream interaction with plasmas (Research monograph no. 29)*. MIT Press.

Chomaz, J. M. 2005 Global instabilities in spatially developing flows: Non-normality and nonlinearity. *Ann. Rev. Fluid Mech.* **37**, 357–392.

Chomaz, J. M., Huerre, P. & Redekopp, L. G. 1988 Bifurcation to local and global modes in spatially developing flows. *Phys. Rev. Lett.* **60**, 25–.

Coenen, W. 2010 Absolute instability in the near field of low-density jets. PhD thesis, Universidad Carlos III de Madrid.

Coenen, Wilfried & Sevilla, A. 2012 The structure of the absolutely unstable regions in the near field of low-density jets. *J. Fluid Mech.* **713**, 123–149.

Cohen, J. & Wygnanski, I. 1987 The evolution of instabilities in the axisymmetrical jet. Part 1. The linear growth of disturbances near the nozzle. *J. Fluid Mech.* **176**, 191–219.

Couairon, A & Chomaz, J. M. 1999 Fully nonlinear global modes in slowly varying flows. *Phys. Fluids* **11**, 3688–3703.

Gaster, M. 1968 Growth of disturbances in both space and time. *Phys. Fluids* **11**, 723–727.

Hallberg, M. P., Srinivasan, V., Gorse, P. & Strykowski, P. J. 2007 Suppression of global modes in low-density axisymmetric jets using coflow. *Phys. Fluids* **19** (1), 014102.

Hallberg, M. P. & Strykowski, P. J. 2006 On the universality of global modes in low-density axisymmetric jets. *J. Fluid Mech.* **569**, 493–507.

Helmholtz, H. von 1868 Über discontinuirliche Flüssigkeitsbewegungen. *Monats. Königl. Preuss. Akad. Wiss. Berlin* **23**, 215–228.

Holmes, M. H. 2007 *Introduction to Numerical Methods in Differential Equations*. Springer, New York.

Huerre, P. 2000 Open shear flow instabilities. In *Perspectives in fluid dynamics* (ed. G. Batchelor, K. Moffatt & G. Worster), pp. 159–229. Cambridge.

Huerre, P. & Monkewitz, P. A. 1985 Absolute and convective instabilities in free shear layers. *J. Fluid Mech.* **159**, 151–168.

Huerre, P. & Monkewitz, P. A. 1990 Local and global instabilities in spatially developing flows. *Annu. Rev. Fluid Mech.* **22**, 473–537.

Jendoubi, S. & Strykowski, P. J. 1994 Absolute and convective instability of axisymmetric jets with external flow. *Phys. Fluids* **6**, 3000–3009.

Kambe, T. 1969 The stability of an axisymmetric jet with parabolic profile. *J. Phys. Soc. Jpn.* **26** (2), 566–575.

Kelvin, Lord 1871 Hydrokinetic solutions and observations. *Phil Mag. (4)* **42**, 362–377.

Khorrami, M. R., Malik, M. R. & Ash, R. L. 1989 Applications of spectral collocation techniques to the stability of swirling flows. *J. Comput. Phys.* **81**, 206.

Kyle, D. M. & Sreenivasan, K. R. 1993 The instability and breakdown of a round variable-density jet. *J. Fluid Mech.* **249**, 619–664.

Landau, L. & Lifschitz, E. M. 1954 *Mechanics of Continuous Media*. Moscow: Fizmatgiz (In Russian).

Lessen, M. & Singh, P. J. 1973 The stability of axisymmetric free shear layers. *J. Fluid Mech.* **60** (3), 433–457.

Lesshafft, L. & Huerre, P. 2007 Linear impulse response in hot round jets. *Phys. Fluids* **19** (2), 024102.

Lesshafft, L., Huerre, P., Sagaut, P. & Terracol, M. 2006 Nonlinear global modes in hot jets. *J. Fluid Mech.* **554**, 393–409.

Mattingly, G. E. & Chang, C. C. 1974 Unstable waves on an axisymmetric jet column. *J. Fluid Mech.* **65** (3), 541–560.

Mollendorf, J. C. & Gebhart, B. 1973 An experimental and numerical study of the viscous stability of a round laminar vertical jet with and without thermal buoyancy for symmetric and asymmetric disturbances. *J. Fluid Mech.* **61** (2), 367–399.

Monkewitz, P. A. 1988 The absolute and convective nature of instability in two-dimensional wakes at low reynolds numbers. *Phys. Fluids* **31**, 999–1006.

Monkewitz, P. A., Bechert, D. W., Barsikow, B. & Lehmann, B. 1990 Self-excited oscillations and mixing in a heated round jet. *J. Fluid Mech.* **213**, 611–639.

Monkewitz, P. A., Lehmann, B., Barsikow, B. & Bechert, D. W. 1989 The spreading of self-excited hot jets by side jets. *Phys. Fluids A* **1** (3), 446–448.

Monkewitz, P. A. & Sohn, K. D. 1988 Absolute instability in hot jets. *AIAA J.* **28**, 911–916.

Morris, P. J. 1976 The spatial viscous instability of axisymmetric jets. *J. Fluid Mech.* **77** (3), 511–529.

Nichols, J. W., Schmid, P. J. & Riley, J. J. 2007 Self-sustained oscillations in variable-density round jets. *J. Fluid Mech.* **582**, 341–376.

Pier, B., Huerre, P., Chomaz, J.-M. & Couairon, A. 1998 Steep nonlinear global modes in spatially developing media. *Phys. Fluids* **10** (10), 2433–2435.

Raghu, S. & Monkewitz, P. A. 1991 The bifurcation of a hot round jet to limit-cycle oscillations. *Phys. Fluids* **3** (4), 501–503.

Rayleigh, Lord 1880 On the stability, or instability, of certain fluid motions. *Proc. London Math. Soc.* **11**, 57–70.

Reynolds, A. J. 1962 Observations of a liquid-into-liquid jet. *J. Fluid Mech.* **14**, 552–556.

Roberts, G. O. 1971 Computational meshes for boundary layer problems. In *Lecture Notes in Physics 8*, , vol. 61, pp. 171–177. Proc. Second Int. Conf. Num. Methods Fluid Dyn., Springer, Berlin.

Sevilla, A. 2011 The effect of viscous relaxation on the spatiotemporal stability of capillary jets. *J.Fluid Mech.* **684**, 204–226.

Sevilla, A., Gordillo, J. M. & Martínez-Bazán, C. 2002 The effect of the diameter ratio on the absolute and convective instability of free coflowing jets. *Phys. Fluids* **14**, 3028–3038.

Sreenivasan, K. R., Raghu, S. & Kyle, D. 1989 Absolute instability in variable density round jets. *Exps. Fluids* **7**, 309–317.

Srinivasan, K., Hallberg, M. P. & Strykowski, P. J. 2010 Viscous linear stability of axisymmetric low-density jets: Parameters influencing absolute instability. *Phys. Fluids* **22**, 024103.

Sturrock, P. A. 1958 Kinematics of growing waves. *Phys. Rev.* **112**, 1488–1503.

Tam, C. K. W. 1971 Directional acoustic radiation from a supersonic jet generated by shear layer isntability. *J. Fluid Mechanics* **46**, 757–768.

Twiss, Q. 1951 On oscillations in electron streams. *Proc. Phys. Soc. (London)* **B64**, 654–669.

Twiss, Q. 1952 Propagation in electron-ion streams. *Phys. Rev.* **88**, 1392–1407.

Yu, M.-H. & Monkewitz, P. A. 1990 The effect of nonuniform density on the absolute instability of two-dimensional inertial wakes and jets. *Phys. Fluids A* **2**, 611–639.